Differences between two estimates of air-sea turbulent heat fluxes over the Atlantic Ocean

A. Santorelli,[1] R. T. Pinker,[1] A. Bentamy,[2] K. B. Katsaros,[3] W. M. Drennan,[3] A. M. Mestas-Nuñez,[4] and J. A. Carton[1]

Received 29 December 2010; revised 20 May 2011; accepted 22 June 2011; published 23 September 2011.

[1] Uncertainties in turbulent ocean-atmosphere heat flux estimates, both among the estimates and between them and ground truth, suggest that further comparisons are needed. We analyze estimates from the French Research Institute for Exploitation of the Sea (IFREMER) and the Woods Hole Oceanographic Institution's Objectively Analyzed air-sea Fluxes (WHOI OAFlux). The IFREMER products are based on satellite observations and the WHOI OAFlux ones on data from satellites, buoys, and ships assimilated into numerical analyses. We focus on the Atlantic sector (70°W–30°E, 45°S–45°N) during 1996–2005, where the variables that enter the bulk formulae for computing fluxes (wind speed, sea surface and air temperature, and specific humidity) can be evaluated against buoys in the Prediction and Research Moored Array in the Atlantic (*PIRATA*). Since WHOI assimilates *PIRATA* observations, we have added two independent buoy data sets: *FETCH* and *ROMEO*. To examine how each variable contributes to the difference between estimated and buoy fluxes, the method of Bourras (2006) is applied. His so-called Q terms showed that specific air humidity and air temperature contributed the most to the biases of IFREMER latent and sensible heat fluxes, respectively, at both independent buoys. For WHOI OAFlux products, deviations from *FETCH* values were mainly due to wind speed and sea surface temperature differences, while in comparison with *ROMEO* fluxes, WHOI OAFlux biases were primarily due to specific humidity and sea surface temperature estimates. Modified estimates of turbulent fluxes with the IFREMER approach using the 10 m specific humidity and air temperature products of Jackson et al. (2009) show significant improvement in three test cases at *PIRATA* buoys.

Citation: Santorelli, A., R. T. Pinker, A. Bentamy, K. B. Katsaros, W. M. Drennan, A. M. Mestas-Nuñez, and J. A. Carton (2011), Differences between two estimates of air-sea turbulent heat fluxes over the Atlantic Ocean, *J. Geophys. Res.*, *116*, C09028, doi:10.1029/2010JC006927.

1. Introduction

1.1. Background

[2] Air-sea heat flux or the exchange of heat between the atmosphere and ocean, controls seasonal variations of sea surface temperature (SST), and, in turn, seasonal to interannual climate variability [*Niiler and Kraus*, 1977; *Houghton*, 1991; *Cayan*, 1992; *Yu et al.*, 2006]. There is also an intraseasonal response in SST to latent heat flux over the ocean interior with the exception of areas of equatorial upwelling, such as the eastern tropical Atlantic cold tongue region [*Grodsky et al.*, 2009]. The impact of air-sea heat flux on SST is also manifested in hurricane intensification, as ocean-to-atmosphere heat fluxes on the order of thousands of watts per meter squared are released when a hurricane moves over warm tropical waters, cooling the upper ocean but warming the atmosphere and producing enhanced convection [e.g., *Shay et al.*, 2000; *Cione and Uhlhorn*, 2003]. Two seasonal to interannual modes of SST variability in the tropical Atlantic that are controlled mainly by latent heat fluxes have impact on American and African climates [*Servain et al.*, 1998]: (1) an equatorial seasonal-interannual mode involving SST anomalies that is akin (but unrelated) to the El Niño-Southern Oscillation events [*Wang et al.*, 2006] and (2) an Atlantic meridional SST gradient mode (5°–25°N, 5°N–20°S) associated with the location and intensity of the ITCZ [*Mestas-Nuñez and Enfield*, 1999]. Accuracy of air-sea heat flux estimates must be optimal for correct observation and modeling of these climatic phenomena.

[1]Department of Atmospheric and Oceanic Science, University of Maryland, College Park, Maryland, USA.
[2]Institut Francais de Recherche pour l'Exploitation de la Mer, Plouzane, France.
[3]Rosenstiel School of Marine and Atmospheric Science, University of Miami, Miami, Florida, USA.
[4]Department of Physical and Environmental Sciences, Texas A&M University-Corpus Christi, Corpus Christi, Texas, USA.

0148-0227/11/2010JC006927

[3] In this article we focus on the turbulent latent and sensible heat fluxes at the air-sea interface, leaving the radiative terms for separate publications, but keeping in mind that all the energy flux terms contribute to net heating or cooling of the upper ocean. The radiative fluxes obtained by satellite measurements at the top of the atmosphere require very different methods of analysis, including radiative transfer modeling, and use a different set of satellite observations. The ultimate goal of our group is, however, to produce a complete data set where all the flux terms have been produced and are fully evaluated and therefore the net flux is well characterized.

[4] Bulk parameterizations of the air-sea turbulent fluxes are used in numerical models as well as with satellite based observations to estimate surface fluxes. These are based on the Monin-Obukhov similarity theory (MOST) to formulate fluxes in terms of mean quantities [*Fairall et al.*, 2003]

$$\overline{w'x'} = c_x^{\frac{1}{2}} c_d^{\frac{1}{2}} S\Delta X = C_x S\Delta X \tag{1}$$

where w' represents vertical velocity, x can be the water vapor specific humidity, q, or potential temperature, θ, and the prime represents deviations from the mean. Here, c_x is the bulk transfer coefficient for the variable x (d being used for the wind speed), and C_x is the total transfer coefficient. Here, ΔX is the air-sea difference in the mean value of x ($\Delta X = X_{sea} - X(z)$), and S is the mean wind speed (relative to the ocean surface). The transfer coefficients depend on surface stability prescribed by MOST

$$c_x^{\frac{1}{2}}(\zeta) = \frac{c_{xn}^{1/2}}{1 - \frac{c_{xn}^{1/2}}{\kappa}\psi_x(\zeta)} \tag{2}$$

$$c_{xn}^{1/2} = \frac{\kappa}{\ln\left(\frac{z}{z_{ox}}\right)} \tag{3}$$

where n refers to neutral stability (when $\zeta = 0$), z is the height of measurement of the mean quantity $X(z)$, ψ_x is an empirical function describing the stability dependence of the mean profile, κ is von Karman's constant, and z_{ox} is the roughness length that characterizes the neutral transfer properties of the surface for x. The MOST stability parameter, ζ, is given as

$$\zeta = \frac{-\kappa g z}{T} \frac{\left(\overline{w'\theta'} + 0.61T\overline{w'q'}\right)}{-\overline{w'u'}^{3/2}} \tag{4}$$

where T is temperature, g is the acceleration due to gravity, and $-\overline{w'u'}$ is the stream-wise component of momentum flux with u representing horizontal velocity.

[5] The bulk parameterizations of latent and sensible heat fluxes are given as

$$LHF = \rho L_V C_E U_A (Q_S - Q_A) \tag{5}$$

$$SHF = \rho c_p C_H U_A (T_S - T_A) \tag{6}$$

where ρ is air density, L_V is the latent heat of vaporization, c_p is the specific heat capacity of air at constant pressure, and Q_A, T_A and U_A are specific humidity, air temperature and wind speed at a specified height above the surface. Q_S and T_S are the specific humidity and temperature at the sea surface; Q_S is assumed to be 98% of the saturation humidity at sea surface temperature; C_E and C_H are moisture and heat exchange coefficients.

1.2. Previous Studies

[6] In previous studies several data sets of turbulent air-sea heat fluxes as well as the variables used to calculate them (air temperature, specific humidity, wind speed, and sea surface temperature) have been evaluated to examine uncertainty of flux estimates.

[7] *Schulz et al.* [1997] compared latent heat fluxes estimated using Special Sensor Microwave/Imager (SSM/I) wind speed and humidity and Advanced Very High Resolution Radiometer (AVHRR) SST data to those made using in situ observations from several field projects in the Atlantic and Pacific (weather-ship M in the Atlantic, the Tropical Ocean Global Atmosphere Program's Coupled Ocean Atmosphere Response Experiment (TOGA-COARE) and the Central Equatorial Pacific Experiment (CEPEX) in the Pacific) as well as a data set of ship/buoy measurements. Differences between satellite and ship/buoy data (instantaneous) are 30 W m^{-2} reduced to 15 W m^{-2} if averaged monthly.

[8] *Josey* [2001] compared fluxes from the National Centers for Environmental Prediction-National Center for Atmospheric Research (NCEP-NCAR) [*Kalnay et al.*, 1996], and the European Centre for Medium-Range Weather Forecasting (ECMWF) [*Gibson et al.*, 1997] to those of WHOI research buoys during the subduction experiment in the Northeast Atlantic (1991–1993; 18°–33°N, 22°–34°W). Net ocean heat gain was underestimated by the re-analyses, due to overestimation of latent heat loss as well as underestimated shortwave radiation gain. Choice of bulk algorithms in the models seemed to be the cause of latent heat biases. Southampton Oceanography Centre (SOC) ship-based fluxes were closer to the buoys' values but still showed some differences (<5 W m^{-2} for sensible, <20 W m^{-2} for latent) fluxes, respectively.

[9] *Smith et al.* [2001] compared NCEP re-analyses to World Ocean Circulation Experiment (WOCE) research vessel observations, and found that NCEP latent and sensible heat fluxes were largely overestimated in the re-analyses. *Kubota et al.* [2003] compared LHF of version 1 of the Goddard Satellite-Based Surface Turbulent Fluxes (GSSTF-1) [*Chou et al.*, 1997], the Hamburg Ocean Atmosphere Parameters and Fluxes from Satellite Data set (HOAPS) [*Grassl et al.*, 2000], the Japanese Ocean Flux Data sets with Use of Remote Sensing Observations (J-OFURO) [*Kubota et al.*, 2002], NCEP and ECMWF re-analyses for 1992–1994 and the *da Silva et al.* [1994] data set over global oceans. They found that large-scale patterns of latent heat flux are similar but that large quantitative differences among various products exist.

[10] *Chou et al.* [2004] compared monthly latent heat flux estimates over the oceans during 1992–1993 using: version 2 of the Goddard Satellite-Based Surface Turbulent Fluxes (GSSTF-2) [*Chou et al.*, 2003], HOAPS, the NCEP reanalysis and the *da Silva et al.* [1994] data set. Large-scale patterns of the 2-year mean 10 m wind speed, 10 m specific humidity and sea-air humidity differences were similar among the data sets, but there were significant quantitative differences. The *da Silva et al.* [1994] data set had large

differences with GSSTF-2 for all variables in the southern extra-tropics. NCEP had low temporal correlation and large differences with GSSTF-2 for sea-air humidity differences in the Tropics (~0.5–1.5 g kg^{-1}). NCEP also exhibited larger latent heat fluxes than GSSTF-2 in the Tropics as well as in the Gulf Stream and Subtropics with a maximum difference of 40 W m^{-2}. In addition, the HOAPS mean latent heat flux was significantly smaller than GSSTF-2 by ~31% (37 W m^{-2}) over the Tropics; HOAPS had systematically smaller latent heat fluxes than GSSTF-2 with a globally averaged difference of 20 W m^{-2}. This difference can be attributed to HOAPS exhibiting smaller 10 m wind speeds than those of GSSTF-2 by up to 2 m s^{-1} as well as larger 10 m specific air humidity values. The other two data sets had large spatial variations of large positive and negative flux differences compared to GSSTF-2 that canceled to produce smaller regional-mean differences.

[11] *Bourras* [2006] compared five monthly satellite products of latent heat flux, including GSSTF-2, the second version of HOAPS [*Fennig et al.*, 2006], J-OFURO, the *Jones et al.* [1999] data set, which is limited to 30°S–30°N, and the Bourras-Eymard-Liu data set (BEL) [*Bourras et al.*, 2002] to ground observations. These included Tropical Atmosphere-Ocean array (*TAO*) buoys, National Data Buoy Center (*NDBC*) buoys off the U.S. coasts, and Met Office/Meteo-France (*UK-MF*) moorings west of United Kingdom and France for the period of 1998–2000. Examination of the deviation between satellite and surface data using bulk variables was performed using an approach where the bulk formula for latent heat flux was differentiated to form "Q terms," or contributions to the deviation between satellite and surface data (in W m^{-2}) for each of the bulk variables (see Appendix A for details).

[12] It was found that all of the satellite data sets except those of *Jones et al.* [1999] had systematic errors ranging from −13 to −26 W m^{-2} and biases of 6–8 W m^{-2} at midlatitudes. In the tropical Pacific, the systematic deviation between latent heat fluxes from the *Jones et al.* data set and *TAO* buoys was 49 W m^{-2}. In this region, it was found that the lack of accuracy in specific air humidity posed problems for satellite flux estimates. The Q term corresponding to differences in specific air humidity was responsible for almost all of the total Q term averaged over all *TAO* buoys for HOAPS-2 (10 W m^{-2}), and the Q terms for specific surface and air humidity contributed 10–15 W m^{-2} each to the uncertainty of GSSTF-2 latent heat fluxes. Note that the *Jones et al.* data set did not provide specific humidity estimates, so no comparison to ground truth was provided.

[13] In addition to uncertainties in flux estimation due to differences in input variables we considered uncertainties due to differences in the formulation of bulk algorithms. *Zeng et al.* [1998] used TOGA COARE ship data and the multiyear hourly TOGA Tropical Atmosphere-Ocean moored buoy data to compare six different algorithms widely used in research, forecasting and data reanalysis. The study showed that algorithms differ significantly in heat and momentum fluxes under both weak and strong winds. Vapor pressure reduction of 2% over saline seawater (used in COARE3.0) has a significant impact on latent heat flux estimates under strong wind conditions. *Chang and Grossman* [1999] compared five bulk flux formulae using the same observations in the COARE region (RV *Moana Wave*; November 1992–February 1993), with a focus on light wind conditions. For most of the algorithms, the bulk flux differed from the covariance flux due to wind speed dependent bias in the model surface flux parameterization. Further error analysis also showed that instrument uncertainties in the inputs to the formulae also contributed to bulk flux errors.

[14] *Brunke et al.* [2002] performed an inter-comparison of eight bulk algorithms for the tropical Pacific and midlatitude Atlantic, including the Coupled Ocean-Atmosphere Response Experiment (COARE) [*Fairall et al.*, 1996], the *Smith* [1988] algorithm used to produce the HOAPS data set, as well as algorithms used in several models and re-analyses. Hourly and monthly flux values were estimated by these eight algorithms using data from several buoy experiments, including the *TAO* array. The results showed significant differences in fluxes due to the handling of the wave spectrum, convective gustiness and salinity as well as roughness length and the parameterization of the turbulent exchange coefficients.

[15] Some algorithms showed deviations from observations under certain conditions; for hourly fluxes, there were large differences in both latent and sensible heat fluxes at weak and strong winds. For wind speeds between 10.75 and 11.25 m s^{-1}, differences among algorithms were as large as ~57 W m^{-2} for latent heat flux and ~3 W m^{-2} for sensible heat flux. Differences in monthly mean latent heat fluxes occurred for very unstable conditions; at an SST of 28° ± 0.25°C, the maximum difference in latent heat flux was ~23 W m^{-2}. Over the tropical Pacific, the maximum average difference in monthly heat flux among algorithms was ~18 W m^{-2}. Over the midlatitude Pacific, algorithms calculated latent heat fluxes that were consistent with observations.

[16] Furthermore, *Brunke et al.* [2003] evaluated twelve bulk aerodynamic algorithms (eight of which were used in the 2002 study) and ranked them by using direct turbulent flux measurements determined from covariance and inertial-dissipation methods from twelve ship cruises over the tropical and midlatitude oceans. The top four algorithms were version 3 of the COARE algorithm (COARE3.0) [*Fairall et al.*, 2003], the University of Arizona scheme [*Zeng et al.*, 1998], the ECMWF algorithm [*Beljaars*, 1995a, 1995b] and the scheme used for version 1 of the Goddard Earth Observing System reanalysis (GEOS-1) [*Chou*, 1993].

[17] *Smith et al.* [2010] carried out a comparison between nine turbulent flux products including momentum as well as latent and sensible air-sea heat fluxes. They included several re-analysis products and two satellite ones, an early version of HOAPS and IFREMER's. They had two flux products based on in situ data, their own from Florida State (FSU) and the National Ocean Center one. This study has in part been super-ceded by recent improvements in several of these products, which they state in their conclusion, but their discussion may still be very helpful for researchers using one of the many re-analysis products. They state in their conclusion, that "no one product is ideally suited for every application," and they give some practical advice on how to make a choice.

1.3. Present Study

[18] In this study, we compare the IFREMER and the WHOI OAFlux data sets to each other as well as to ground truth from several field programs for the period of 1996–2005 to understand the reasons for their differences. The

Table 1. Variables Used to Derive IFREMER and WHOI OAFlux Turbulent Heat Fluxes (Latent and Sensible) and Their Origin

Variable	Source for IFREMER	Source for WHOI OAFlux
Air temperature	Estimated from specific air humidity, wind speed and sea surface temperature using the *Konda et al.* [1996] model	NCEP, ECMWF re-analyses
Sea surface temperature	*Reynolds et al.* [2007]	NCEP, ECMWF re-analyses, *Reynolds et al.* [2007]
Surface wind speed	ERS-1, ERS-2, QuickSCAT scatterometers SSM/I wind speed	NCEP, ECMWF re-analyses, SSM/I and AMSR-E radiometers, QuickSCAT scatterometer
Specific air humidity	Estimated from SSM/I brightness temperature using the *Bentamy et al.* [2003] model	NCEP, ECMWF re-analyses, product from *Chou et al.* [1997] using SSM/I column water vapor retrievals

variables that enter the computations of the fluxes, such as sea surface and air temperature, wind speed, and specific humidity, are also compared. In section two we discuss the data sets included in the comparison. Section three discusses the comparison methodology. In section four, the spatial and temporal differences in latent and sensible heat fluxes are presented, followed by a qualitative and quantitative discussion of the input variables. Each component is compared to independent "ground truth" from the field experiments. In this section we also present test cases, where the *Jackson et al.* [2006, 2009] method for obtaining atmospheric specific humidity and air temperature have been used in the IFREMER computations. In section five we summarize our findings and discuss how this study can contribute to a better understanding of air-sea heat flux differences.

2. Data Sets

[19] The IFREMER data are available at http://cersat.ifremer.fr/layout/set/print/news/products_informations/new_release_of_satellite_turbulent_fluxes_1992_2007 [*Bentamy et al.*, 2008] as weekly and monthly estimates on a 1° × 1° (latitude × longitude) spatial grid. The WHOI OAFlux data are available for years 1985–2010 as daily estimates on a 1° × 1° spatial grid [*Yu et al.*, 2008]. Table 1 lists each variable used to calculate latent and sensible heat fluxes for IFREMER and WHOI OAFlux and the sources of the information. Each meteorological input variable and resulting flux term will be discussed separately.

2.1. SST

[20] Both IFREMER and WHOI use the most recent release of the Reynolds SST analysis [*Reynolds et al.*, 2007]. The data have a 0.25° horizontal resolution at daily time scale. WHOI utilized the Reynolds SST product based on the Advanced Very High Resolution Radiometer (AVHRR) infrared observations for January 1985–December 2005; IFREMER uses the same product through 2002 and AVHRR data merged with the Advanced Microwave Scanning Radiometer-Earth Observing System (AMSR-E) data from 2002 onward. Both versions of the Reynolds SST data set are subjected to optimal interpolation (OI). In addition to the satellite SST retrievals from AVHRR and AMSR-E, the Reynolds products assimilate observations from ships and buoys from the International Comprehensive Ocean-Atmosphere Data Set (ICOADS). For the marginal ice zone, sea ice data from microwave satellite data by *Grumbine* [1996] with delayed sea ice concentrations by *Cavalieri et al.* [1999] are used to mask the ice edge. IFREMER and WHOI OAFlux interpolated the Reynolds data set to 1° resolution.

[21] In addition to the Reynolds SST data set, WHOI also utilized SST values from re-analyses by the European Centre for Medium Range Forecasting 40-Year Reanalysis (ERA-40) project [*Beljaars and Kallberg*, 2001] and from NCEP [*Kistler et al.*, 2001]. The ECMWF system consists of a forecast model at T59 resolution (125 km horizontal resolution, with 60 vertical levels up to 64 km) and a three-dimensional variational data assimilation scheme with six-hour intervals. The observations used to derive the reanalysis includes in situ data from ICOADS, ship observations and radiosondes, as well as satellite radiances from TOVS (TIROS Operational Vertical Sounder) water vapor data from the Special Sensor Microwave/Imager (SSM/I) and wind data from scatterometers. Sea surface temperatures and sea-ice interface are prescribed from the United Kingdom Meteorological Organization Hadley Centre (HadISST1) monthly SST and ice limit analyses and the NCEP (2DVAR) weekly SST and ice limit analysis.

[22] The SST data from the re-analyses are re-gridded by WHOI to 1° resolution for ease of synthesis with the Reynolds SST data through objective analysis (used for all surface meteorological variables and fluxes); this analysis is based on the Gauss-Markov theorem, which states that the linear least squares estimator is the most efficient estimator when combining data linearly, with the solution of minimum variance. *Yu et al.* [2008] performed error estimation between analysis and in situ observations using the National Oceanographic Centre (NOC) surface meteorology and air-sea heat flux ship measurement climatologies as well as buoy measurements from the WHOI Improved Meteorological instruments (*IMET*) [*Moyer and Weller*, 1997], the *TAO/TRITON* buoy array in the tropical Pacific [*McPhaden et al.*, 1998] and in the Indian Ocean [*McPhaden et al.*, 2006], and the Pilot Research Moored Array in the Tropical Atlantic (*PIRATA*) [*Servain et al.*, 1998]. An assumption was made that NOC data errors were several times smaller than those of Numerical Weather Prediction, making the error covariance of NOC data negligible. This error information was used to determine weights that indicate how each data set used in the WHOI OAFlux product (ERA40, NCEP1, NCEP2 and satellite) contributed to the final estimate of air-sea fluxes and flux parameters. ERA40 specific air humidity and air temperature had larger weights assigned to them than values from both NCEP re-analyses, and satellite SST and wind speed made greater contributions compared to those of re-analyses.

2.2. Specific Air Humidity

[23] IFREMER uses an empirical model relating SSM/I brightness temperatures to the specific air humidity at 10 m [*Bentamy et al.*, 2003; *Schulz et al.*, 1993, 1997]. Brightness

temperatures were provided by the Marshall Space Flight Center. WHOI applied the *Chou et al.* [1995, 1997] algorithm to SSM/I precipitable water and field humidity soundings from the ocean at 10 m height, which is a second-order approximation of the EOF expansion for the specific humidity profile; this was deemed appropriate because the first EOF is related to total precipitable water, and the second EOF is related to the fraction of precipitable water in the PBL. The SSM/I humidity was first height-adjusted from 10 m to 2 m based on version 3.0 of the Coupled Ocean Atmosphere Research Experiment (COARE3.0) [*Fairall et al.*, 2003] algorithm. WHOI OAFlux estimation also used values for 2 m specific humidity from the NCEP and ECMWF re-analyses and applied advanced objective analysis to the inputs.

2.3. Surface Wind Speed

[24] IFREMER winds are mainly derived from scatterometers onboard the European Remote Sensing satellites 1 and 2 (ERS-1 and ERS-2), the Advanced Earth Observing Satellite 1 (ADEOS-1) and QuikSCAT. To enhance the sampling of surface wind speed at grid points where no scatterometer retrievals are available, winds were estimated with brightness temperatures from SSM/I onboard F11, F13, F14, and F15 as inputs into an algorithm published by *Bentamy et al.* [1999]. Both radar and radiometer retrievals are used to estimate daily averaged winds over the global ocean with spatial resolution of 1° in longitude and latitude. Similar to IFREMER, WHOI OAFlux uses QuikSCAT and version 6 of the Special Sensor Microwave/Imager (SSM/I) data. The algorithm used to derive the SSM/I data [*Wentz*, 1997] relates wind speed to brightness temperature computed from the 37 GHz horizontal and vertical polarized radiance measurements and to the radiative transfer and absorption between the sea surface and satellite. The data used were 12-hourly at a swath resolution of 25 km. Wind speeds were flagged if cloud/rain liquid water values exceeded 18 mg cm^{-2} because the accuracy of wind speed retrievals degrades if rain is present. Wind speed values were also flagged if measurements are within 50–100 km of the coast or within 200 km of the climatological monthly mean position of the ice edge. In addition to the sources cited, WHOI also utilizes AMSR-E data as well as data from NCEP and ECMWF re-analyses. A variational method is applied to the data, which is subjective due to the determination of weights. Wind measurements from both IFREMER and WHOI OAFlux are converted to the equivalent wind speed at 10 m height and to neutral stratification.

2.4. Air Temperature

[25] IFREMER uses specific humidity, surface wind speed and sea surface temperature as inputs to calculate air temperature following *Konda et al.* [1996]

$$q_s - q_a - (C_H/C_E)(T_s - T_a)(A + B) = 0 \tag{7}$$

$$A = \frac{q_a}{Q_*(T_a)}\left(\frac{\partial Q_*(T)}{\partial T}\ at\ T = T_a\right) \tag{8}$$

$$B = Q_*(T_a)\left(\frac{\partial \alpha}{\partial T}\ at\ T = T_a\right) \tag{9}$$

where q_s and q_a are specific surface and air humidity, α is relative humidity, C_H and C_E are heat and moisture transfer coefficients, T_s and T_a are sea surface and air temperatures, and $Q_*(T)$ is the saturation specific humidity curve, which is determined by transformation of the saturation vapor pressure curve. This method utilized two definitions of the Bowen ratio using flux profile as well as bulk formulas to represent sensible and latent heat fluxes. IFREMER air temperature values are adjusted to 10 m height using COARE3.0.

[26] The WHOI data set utilized values for air temperature from NCEP and ECMWF re-analyses at 2 m height and applied advanced objective analysis to the data; the analysis of air temperature was processed from September 1, 2002 to December 31, 2006 using the ERA-interim reanalysis [*Berrisford et al.*, 2009] to replace NCEP. This was done because it was found that NCEP caused Gibbs-like phenomena, or a spurious oscillation of over- and under-shooting that arises due to the use of an eigenfunction series at a simple discontinuity over the ocean near steep orography [*Navarra et al.*, 1994]; this phenomena has been found to affect surface flux estimation since Gibbs oscillations can interact and cause problems with physical parameterizations. The ERA-interim reanalysis uses cycle 31r2 of ECMWF's Integrated Forecast System (IFS), with 60 vertical levels, T255 spherical-harmonic representation for dynamical fields, and a reduced Gaussian grid with approximately uniform 79 km spacing for surface and other grid point fields.

2.5. Turbulent Flux Calculation

[27] To obtain turbulent fluxes, both groups utilize the Coupled Ocean Atmosphere Research Experiment version 3.0 algorithm (COARE3.0) [*Fairall et al.*, 2003]. Although COARE3.0 incorporates sub-models that represent the millimeter-scale cool skin near the interface, the IFREMER implementation does not include this feature. IFREMER used a constant value for surface pressure, while WHOI used a surface pressure field and applied an advanced objective analysis scheme to the data in Table 1 before it was used as input in COARE3.0, as discussed in section 2.1. *Fairall et al.* [2003] stated that, for wind speeds greater than 5 ms^{-1}, surface waves are dominant in affecting surface roughness of the ocean. Two recent parameterizations [*Taylor and Yelland*, 2000; *Oost et al.*, 2002] that allow the Charnock parameter or velocity roughness length to be calculated from wave parameters were incorporated into COARE3.0. The wave models in COARE3.0 were turned off by IFREMER in the flux estimate formulation, while WHOI OAFlux utilized them.

3. Methods

[28] To examine differences among data sets daily, monthly and seasonal estimates of each flux component are used for 1996–2005 in a sector of the Atlantic Ocean (70°W–30°E, 45°S–45°N). The comparisons of the gridded fields are done with each other as well as with independent in situ data from buoys (*PIRATA*/*FETCH*/*ROMEO*). Bias, root-mean-square difference (RMSD), and correlation among data sets for each component are calculated. For the three buoy data sets, in order to examine the deviation between the air-sea flux estimates and the independent ground truth, the "Q term" approach of *Bourras* [2006] is applied to both latent and sensible heat fluxes.

[29] We use buoy measurements from the Prediction and Research Moored Array in the Atlantic (*PIRATA*) [*Servain et al.*, 1998] as ground truth. The *PIRATA* project began in 1997 utilizing Autonomous Temperature Line Acquisition System (ATLAS) moorings, with multivariate measurements, and a real-time data stream submission. Measurements below the surface are transmitted to a processor on the surface buoy from sensors inductively coupled to the mooring line, and all data are relayed to shore via the Service Argos satellite system. The placement of the buoys was chosen to provide coverage along the Equator for regions of strong wind forcing in the western part of the basin and significant seasonal-inter-annual variability in SST in the central and eastern parts of the basin. *PIRATA* buoys provide wind speed at 4 m and air temperature and specific air humidity at 3 m height.

[30] Since the *PIRATA* data are assimilated into the WHOI OAFlux product via error estimation (see section 2), evaluation of the WHOI OAFlux product against such in situ data is not independent. Therefore, independent buoy observations that have not been assimilated into the WHOI products will be also used. In particular, data from two deployments of the University of Miami ASIS (Air-Sea Interaction Spar) buoys [*Graber et al.*, 2000] were utilized. An ASIS buoy was moored in the western Mediterranean (42°58′56″N, 4°15′11″E) during the "flux, etat de la mer, et télédétection en conditions de fetch variable" (*FETCH*) experiment [*Hauser et al.*, 2003]. The overall objective of the *FETCH* experiment was to develop and evaluate methods for estimating turbulent fluxes of heat and momentum at the air-sea interface, and to analyze the turbulent and radiative fluxes in coastal regions and their relation to the atmospheric boundary layer. Observations were collected between March 18 and April 10, 1998 every 28.5 min, but averaged daily for the comparison with the satellite fields. The buoy provides surface wind speed at 7 m, sea surface temperature at 2 m below the surface, as well as air temperature and specific air humidity (calculated from relative humidity) at 5 m. See *Drennan et al.* [2003] for details. A second independent source of observations is the ASIS buoy *ROMEO* [*Zhang et al.*, 2009]. This buoy was deployed at 36°28.4′N, 75°15.3′W as part of the Shoaling Waves Experiment (*SHOWEX*). The buoy is influenced by the Gulf Stream, a region of large discrepancy between IFREMER and WHOI flux estimates; thus, the *ROMEO* data are important for verification in this region. The objective for the deployment of *ROMEO*, as well as the two other ASIS buoys moored during *SHOWEX*, was to measure the evolution of surface waves as well as air-sea fluxes of buoyancy and momentum and mean shelf meteorology. The data set spans October 22–November 30, 1999 at 20-min intervals; the data were averaged at daily time scales to facilitate comparison with the IFREMER and WHOI fluxes. The buoy provides surface wind speed at 6 m, sea surface temperature at 5 m depth, as well as air temperature and humidity at 4.5 m.

[31] The measurement height of certain variables is different among data sets. IFREMER estimates variables at 10 m while WHOI uses air temperature and specific humidity data at 2 m and wind speed at 10 m; these data are in both cases from the advanced objective analysis as applied to the original data. Furthermore, as stated above, buoy values of air-sea flux variables are measured at different heights in each of the four cases. To ensure consistency, we used COARE3.0 to make the proper height adjustments to 10 m for specific air humidity, wind speed and air temperature.

4. Results

4.1. Comparison Between IFREMER and WHOI

4.1.1. Spatial Scale

[32] As evident from Figure 1a, within the Atlantic basin, the IFREMER-WHOI OAFlux 1996–2005 annual mean difference in latent heat flux is positive in the Tropics, with a maximum of 60 W m^{-2} off the Brazilian coast. In a region just off the western African coast (30°S–0°N, 15°W–15°E), there is a dipole of negative (between −20 and 0 W m^{-2}) and positive (≥30 W m^{-2}) difference between the two latent heat flux products. There is a band of negative differences between 45° and 30°S with an area ≤−40 W m^{-2} off the South African coast. In the Gulf Stream region (30°–45°N, 70°–40°W), there are also negative differences of up to −40 W m^{-2}. As seen from Figure 1b, the IFREMER-WHOI OAFlux 1996–2005 annual mean difference in sensible heat flux is positive in most of the Atlantic basin. Around 45°–30°S, IFREMER sensible heat fluxes exhibit the largest difference from WHOI OAFlux (≥30 W m^{-2}); there is also a small area of positive differences of 20–40 W m^{-2} just off the western shore of South Africa (30°–15°S, 15°E). A region where IFREMER sensible heat fluxes were smaller than those of WHOI is in the Gulf Stream region (≤−20 W m^{-2}).

[33] Sea surface temperature differences between IFREMER and WHOI OAFlux are mostly small, except in the Gulf Stream region where they exceed 2°C (Figure 1c); this could be due to gridding concerns in this area of a large SST gradient as well as the fact that WHOI OAFlux used SST from re-analyses in addition to satellite data. Differences in specific air humidity contribute to latent heat flux discrepancies in all regions (note the similarities between Figures 1a and 1d, keeping in mind that a negative bias in specific humidity produces a positive bias in latent heat flux). These differences are negative in the Tropics, with a maximum of −1.5 g kg^{-1} off the Brazilian coast and positive within the 45°–30°S belt (0–0.5 g kg^{-1}) and the Gulf Stream, where there is a maximum difference equal to or exceeding 1.5 g kg^{-1}. There is a clear dipole of positive and negative differences between IFREMER and WHOI OAFlux specific air humidity off the western African coast.

[34] IFREMER wind speeds (Figure 1e) are higher than those of WHOI OAFlux in the Tropics but lower in the Gulf Stream and between 30° and 10°S, where differences are as high as −1 m s^{-1}. These wind speeds contribute to the differences in latent heat fluxes in these regions except for a larger IFREMER latent heat flux off the southern African coast. Differences in sensible heat flux are likely due to contrasts in air temperature between the two data sets (Figure 1f) which are between −1 and 0°C north of the Equator, and between −2 and −1°C south of the Equator. Along ~45°S, the differences are between −4 to −2°C. In the Gulf Stream region, IFREMER air temperature is larger by ≥2°C, but, since sea surface temperature differences are similar, the effect of air temperature may not be as strong as the effect of wind speed in this region.

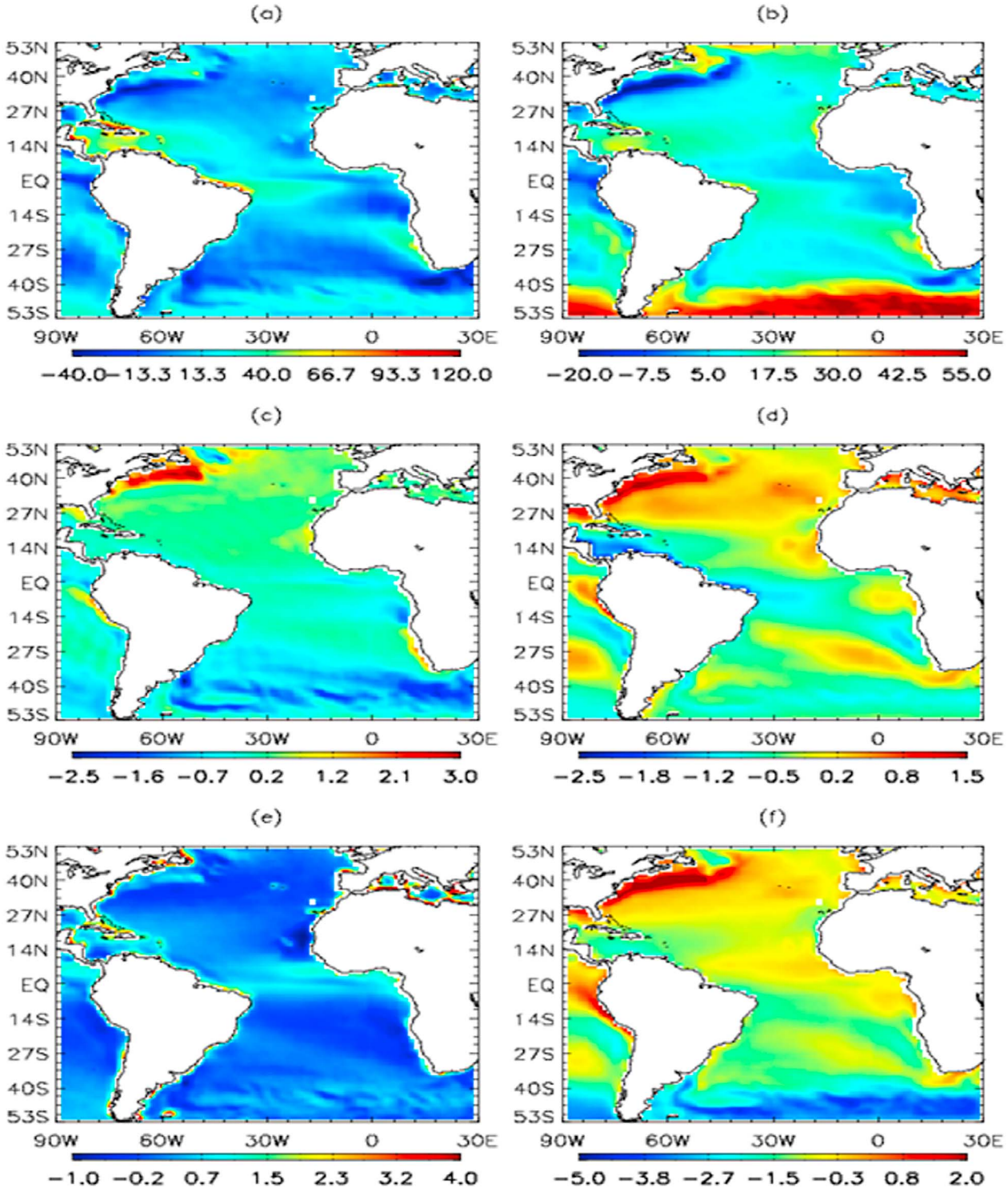

Figure 1. The 1996–2005 annual mean difference IFREMER minus WHOI OAFlux for (a) latent heat flux, (b) sensible heat flux, (c) SST, (d) specific air humidity, (e) surface wind speed and (f) air temperature. Units are W m^{-2} for latent and sensible heat flux, °C for sea surface and air temperature, g kg^{-1} for specific air humidity and m s^{-1} for surface wind speed.

[35] At seasonal time scale, the strong negative difference in latent heat flux in the Gulf Stream vanishes in the summer months, and the area of negative difference off the West African coast appears to move northward into the Equator and narrows (not shown). However, both the area of negative differences off the South African coast and the area of positive differences along the Brazilian coast persist year-round. These correspond to seasonal differences of opposite

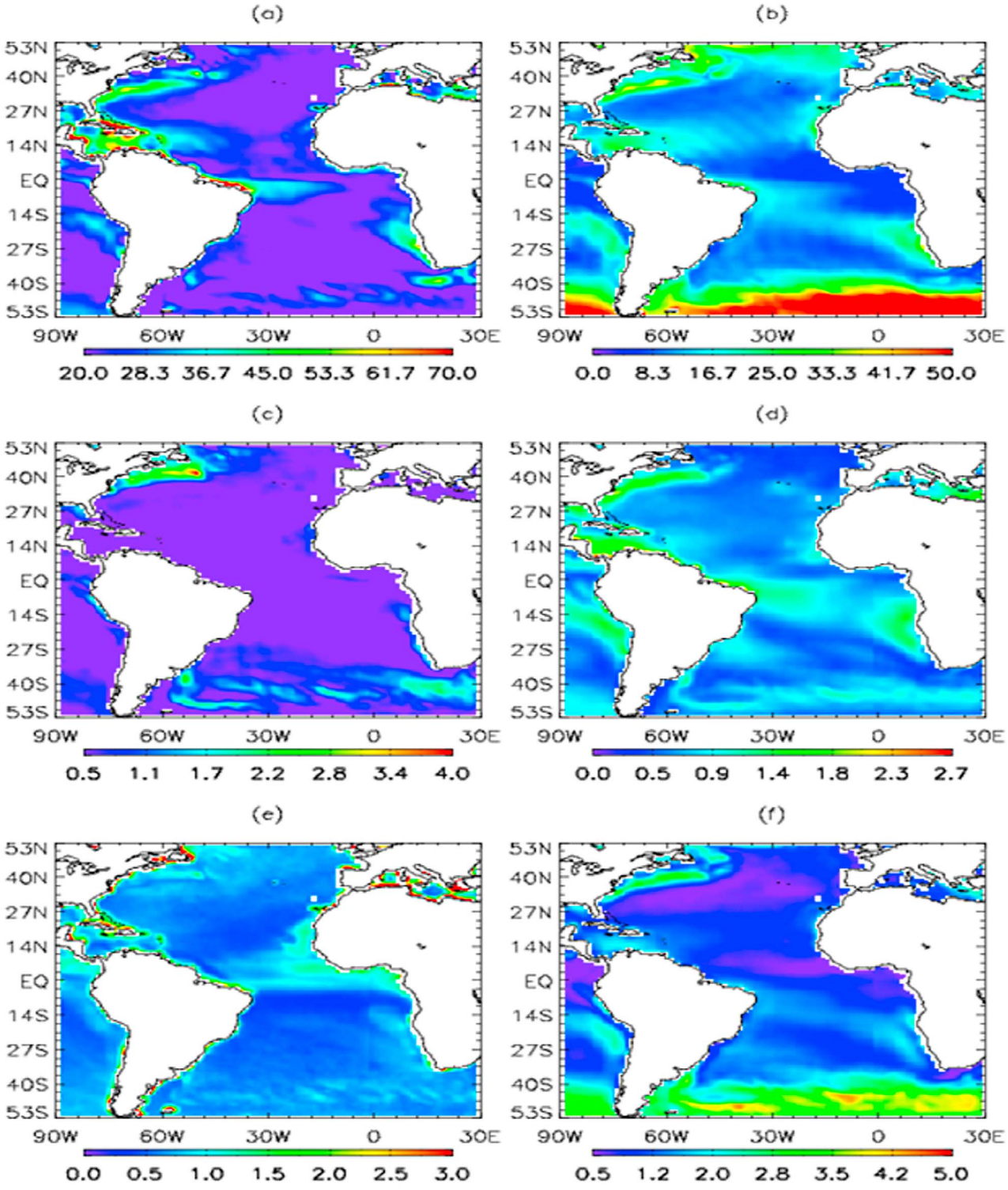

Figure 2. The 1996–2005 annual RMSD between IFREMER and WHOI OAFlux for (a) latent heat flux, (b) sensible heat flux, (c) SST, (d) specific air humidity, (e) surface wind speed and (f) air temperature. Units are W m^{-2} for fluxes, °C for sea surface and air temperature, g kg^{-1} for specific air humidity and m s^{-1} for surface wind speed.

sign for specific air humidity. In the Gulf Stream, it appears that the wind speed difference weakens to between −0.5 and 0 ms^{-1} during the summertime; this coincides with a shift in differences in latent and sensible heat fluxes from very negative to slightly positive (0–20 W m^{-2}) during the same season. The alternation of negative and positive sensible heat flux differences along the West African coast during

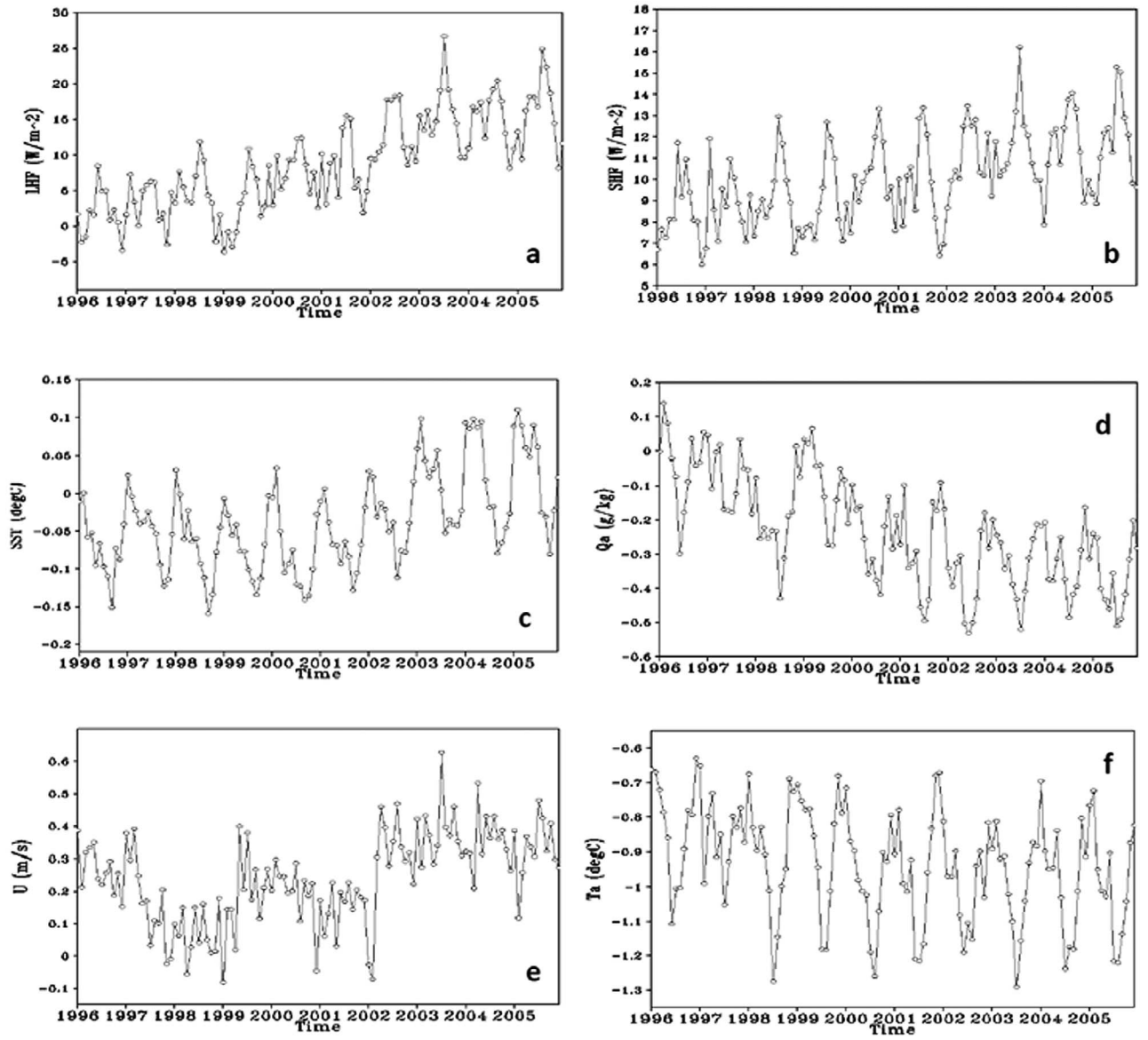

Figure 3. Time series of IFREMER minus WHOI OAFlux monthly data averaged over the Atlantic basin (70°W–30°E, 45°S–45°N) for (a) latent heat flux, (b) sensible heat flux, (c) sea surface temperature, (d) specific air humidity, (e) surface wind speed and (f) air temperature during 1996–2005.

the summer and fall seasons coincide with air temperature differences of the opposite sign.

[36] The root-mean-square difference of latent heat flux between the two data sets (Figure 2a), is highest in the Gulf Stream region, along the northern coast of South America and along the coast of South Africa; RMSD in these regions is ≥40 W m^{-2}. The RMSD of sensible heat flux between the two data sets (Figure 2b) is typically around 10 W m^{-2} but reaches up to 45 W m^{-2} in the Gulf Stream and in the 45°–40°S belt. Also, the RMSD of the bulk variables, including sea surface temperature (Figure 2c; reaching a maximum over 4°C in the Gulf Stream region), specific air humidity (Figure 2d; differences up to 1.8 g kg^{-1} in the Gulf Stream), wind speed (Figure 2e; 1–1.5 m s^{-1} in the 45°–30°S region) and air temperature (Figure 2f; up to 3.5°C in the Gulf Stream region, and up to 4.5°C at 45°–30°S) are shown.

4.1.2. Temporal Comparison

[37] An analysis of the 1996–2005 IFREMER minus WHOI OAFlux temporal differences for the latent and sensible heat fluxes and their associated input variables was also performed. This is summarized in Figures 3 and 4 and Table 2 which include the time series of differences for both the entire basin and zonal belts as well as the overall time-mean difference.

[38] The monthly mean differences averaged over the basin for latent and sensible heat fluxes are 8.9 and 10.1 W m^{-2}, respectively (Table 2). For latent heat flux, the difference is largest in the northern tropical Atlantic (0°–15°N), while sensible heat flux differences are largest in the 15°–30°N and 45°–30°S belts. Note that there is an upward trend in the time-mean latent heat flux difference basin-wide (Figure 3a); the separate time series of basin-averaged IFREMER and

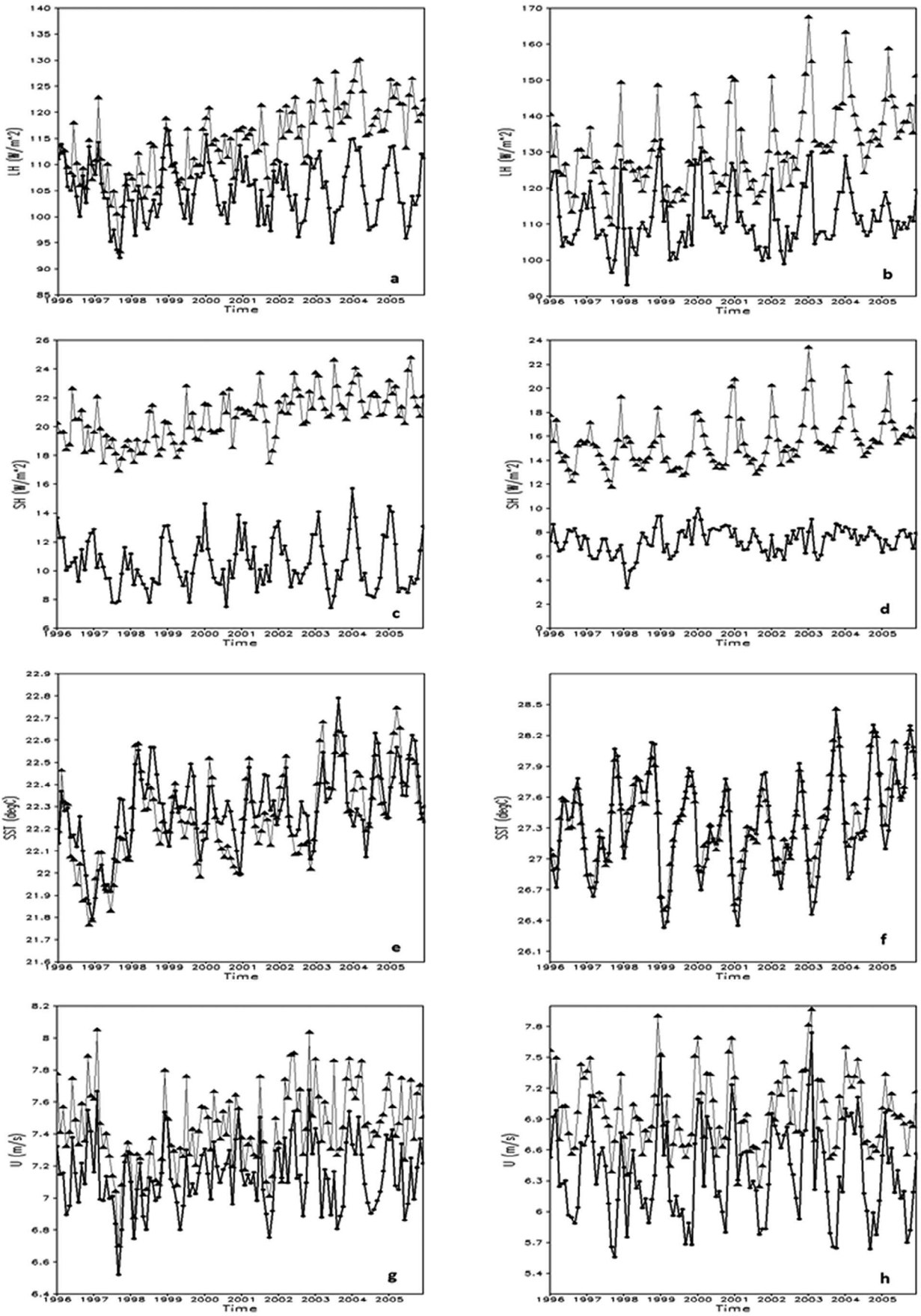
LH (W/m^2)
SH (W/m^2)
SST (deg°)
U (m/s)
Time
1996 1997 1998 1999 2000 2001 2002 2003 2004 2005
a
b
c
d
e
f
g
h

Figure 4

Table 2. Monthly Averaged Difference Between IFREMER and WHOI OAFlux Fluxes and Associated Parameters[a]

Region	MAD LHF 1996–2005 (W m^{-2})	MAD SHF 1996–2005 (W m^{-2})	MAD SST 1996–2005 (°C)	MAD Q_a 1996–2005 (g kg^{-1})	MAD U 1996–2005 (m s^{-1})	MAD T_a 1996–2005 (°C)
Basin-wide	8.9	10.1	0.0	−0.2	0.2	−0.9
30°–45°N	4.2	6.1	0.6	0.4	0.4	0.0
15°–30°N	13.8	12.3	0.3	−0.1	0.2	−0.9
0°–15°N	19.0	8.2	0.1	−0.4	0.6	−0.7
15°S–0°N	13.5	8.8	−0.2	−0.6	0.2	−1.0
30°–15°S	8.8	11.5	−0.1	−0.4	−0.1	−1.2
45°–30°S	−1.8	13.4	−0.7	−0.4	0.2	−1.7

[a]Monthly averaged difference (MAD), latent and sensible heat fluxes (LHF, SHF), sea surface temperature (SST), specific air humidity (Q_a), surface wind speed (U) and air temperature (T_a). for 1996–2005 averaged over the basin (70°W–30°E, 45°S–45°N) and over zonal belts between 70°W and 30°E.

WHOI fluxes show that IFREMER, not WHOI, had the upward trend in monthly averaged latent heat flux (Figure 4a). Examination of the separate time series for each zonally averaged latitudinal belt showed that the basin-averaged time series for this variable were very similar to those of 0°–15°N (Figure 4b).

[39] To explore the causes of the differences between the two data sets, we evaluate the variables that go into the calculation of the fluxes. The time-mean difference in specific air humidity between the two data sets over the basin is −0.2 g kg^{-1} (Table 2); this corresponds to a larger IFREMER latent heat flux. The largest negative differences in specific air humidity lie in the southern tropical Atlantic (15°S–0°N), close to the region where IFREMER latent heat fluxes show the highest values when compared to those of WHOI OAFlux. In Figure 3e, there is a noticeable jump in the time-mean difference in wind speed between the two data sets around 2002; looking at individual time series, IFREMER wind speeds show this jump, but those of WHOI do not (Figure 4g). The difference between IFREMER and WHOI OAFlux wind speeds averaged over the Atlantic basin for 1996–2005 is 0.2 m s^{-1}, and the largest differences occur in the 0°–15°N region (Table 2).

[40] Similar to what is observed in latent heat flux difference, there is also an upward trend in the basin-averaged sensible heat flux difference between the two data sets (Figure 3b). Again, when looking at each data set separately, IFREMER shows the upward trend (Figure 4c), and the 0°–15°N belt is where the trend is most prevalent. IFREMER's sensible heat fluxes exhibits a much larger seasonal cycle than do those of WHOI OAFlux (Figure 4d). For sensible heat flux, variables used in the calculation are sea surface temperature, wind speed and air temperature. Averaged over the Atlantic basin, the time-mean difference between IFREMER and WHOI OAFlux SST is negligible (Table 2), so SST cannot explain IFREMER's higher sensible heat fluxes. Note that there is a sudden increase in the basin-averaged time series of differences in SST between the two data sets around 2002 (Figure 3c); the data sets appear to differ more after this time, and it is particularly evident in the 0°–15°N belt (Figures 4e and 4f). This likely reflects the fact that the WHOI OAFlux product used the AVHRR-only version of the *Reynolds et al.* [2007] satellite SST product for the entire time period, while IFREMER switched to the merged AVHRR/AMSR-E version of the product starting in 2002. Similarly, the negative differences between IFREMER and WHOI wind speed that exist in belts pole-ward of 15°S would not explain the higher sensible heat flux from the IFREMER data. The time-mean basin-averaged difference in air temperature between the two data sets, −0.9°C, would correspond to a higher sensible heat flux for IFREMER (Table 2).

4.2. Comparison of IFREMER and WHOI Products to Ground Truth

4.2.1. Comparison to *PIRATA* Buoys

[41] Each of the input variables used in computations with both data sets were compared to ground truth, first against *PIRATA* buoys. In Table 3, daily values of latent and sensible heat fluxes as well as the variables that enter the bulk formulae were compared to daily averaged estimates from 13 *PIRATA* buoys during 1996–2005. For all variables and fluxes, WHOI OAFlux data had a smaller mean bias and stronger correlation when compared with *PIRATA* data. This is expected since the WHOI data set used *PIRATA* buoys as well as buoys from *IMET* and *TAO* to tune the amplitude of error variances that were constructed based on the use of the NOC air-sea flux and surface meteorology analysis, as mentioned in section 2 [*Yu et al.*, 2008]. Hence this is not a true validation of the WHOI products. Also, some scatter found in daily IFREMER and buoy data comparisons are related to the ability to determine the specific air humidity and from that the air temperature from one or two microwave brightness temperature measurements per day. This limited sampling and the indirect evaluation of air temperature are the main reasons why IFREMER flux data are only made available as weekly and monthly averaged products.

[42] The IFREMER and WHOI OAFlux products showed mean latent heat flux biases of +9.2 and −7.1 W m^{-2} respectably when compared to the *PIRATA* data. That the two biases are so close is remarkable given that the WHOI product assimilate the data while the IFREMER one does not. The mean biases in sensible heat flux are +10.1 and +1.7 W m^{-2}, respectively. IFREMER and WHOI SST data both exhibited low biases and correlations near +1 when compared to *PIRATA* data; IFREMER air-sea fluxes and

Figure 4. Time series of 1996–2005 monthly values for IFREMER (solid triangles) and WHOI OAFlux (solid circles, bold line) averaged over the Atlantic basin (Figures 4a, 4c, 4e, and 4g) and over the 0°–15°N zonal belt (Figures 4b, 4d, 4f, and 4h) for (a, b) latent heat flux (LH), (c, d) sensible heat flux (SH), (e, f) SST and (g, h) surface wind speed (U).

Table 3. Bias, Root-Mean-Square Difference and Correlation Coefficient Calculated Between Daily *PIRATA* Buoy Data and IFREMER, WHOI OAFlux Data During 1996–2005[a]

Variable	IFREMER Bias	WHOI Bias	IFREMER RMSD	WHOI RMSD	IFREMER r	WHOI r
LHF (W m^{-2})	9.2	−7.1	31.7	23.0	0.7	0.8
SHF (W m^{-2})	10.1	1.7	12.3	4.2	0.2	0.6
SST (°C)	−0.1	−0.0	0.4	0.4	1.0	1.0
Q_a (g kg^{-1})	−0.3	−0.1	0.8	0.6	0.9	1.0
U (m s^{-1})	0.3	0.2	1.4	0.7	0.6	0.9
T_a (°C)	−1.0	−0.1	1.1	0.5	0.9	1.0

[a]Root-mean-square difference (RMSD) and correlation coefficient (r). *PIRATA* buoys included in these comparisons are located at 0°N, 0°E; 0°N, 10°W; 0°N, 23°W; 0°N, 35°W; 10°S, 10°W; 4°N, 38°W; 8°N, 38°W; 12°N, 38°N; 15°N, 38°W; 6°S, 10°W; 19°S, 34°W; 2°N, 10°W and 8°S, 30°W. There were a total of 1777 observations available for comparisons among these buoys for each variable (except for SST, which had 2591) during 1996–2005.

WHOI OAFlux products both use the *Reynolds et al.* [2007] satellite SST data set but in different ways as discussed in section 2. In addition, WHOI assimilated SST values from *PIRATA* buoys into their estimates. IFREMER air temperature also had a strong correlation with those of *PIRATA* buoys, but one must note that sensible heat fluxes from each data set correlate poorly due to the difference between SST and air temperature. It is not necessarily realistic, even though each of those two variables show good statistical small errors compared to buoy data, since their deviations from the true values are not generally correlated with each other.

4.2.2. Comparison to the *FETCH* Buoy

[43] Since WHOI uses the *PIRATA* data as part of its assimilation process, it is of interest to evaluate the performance of the two products against observations that were not used by WHOI. Such independent observations are available from the *FETCH* buoy. As seen in Figure 5 and Table 4, IFREMER latent heat fluxes exhibit a negative bias compared to *FETCH* fluxes of −9.1 W m^{-2}, but sensible heat fluxes are positively biased by 9.7 W m^{-2}; the WHOI OAFlux latent heat flux bias was −3.5 W m^{-2}, while the sensible heat flux bias was only −0.5 W m^{-2}.

[44] The analysis of the Q terms for the IFREMER-*FETCH* comparison shows that the observation-averaged Q_{Q_A} (−15.9 W m^{-2}) contributes the most to the total uncertainty term for IFREMER latent heat fluxes, and Q_{T_A} (7.7 W m^{-2}) contributes the most to the total uncertainty term for IFREMER sensible heat fluxes (Table 5). These results correspond to the positive bias in specific air humidity and negative bias in air temperature from the IFREMER data. For the Q term analysis for WHOI-*FETCH*, Q_{U_A} contributes the most to the negative latent heat flux bias (−9.7 W m^{-2}).

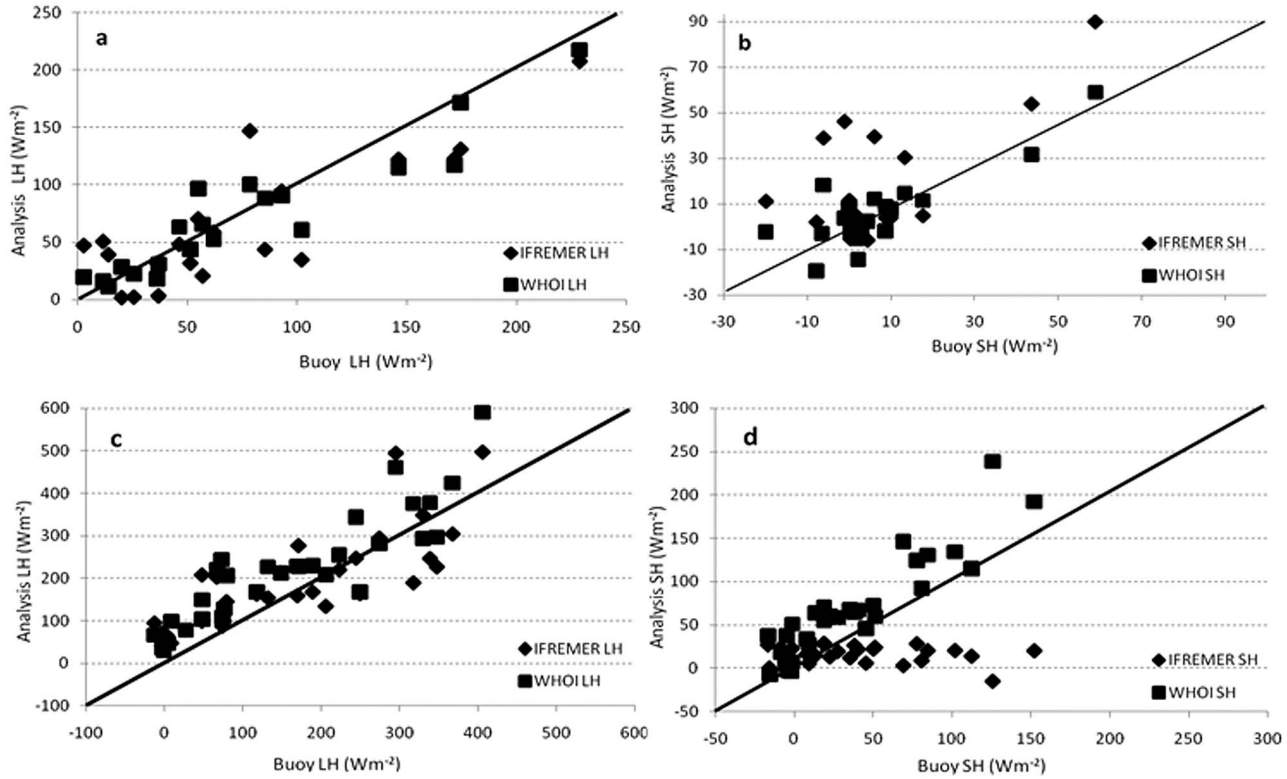

Figure 5. Scatterplots of daily WHOI OAFlux and IFREMER latent heat (LH) and sensible heat (SH) flux values versus (a, b) *FETCH* buoy (42°58′56″N, 4°15′11″E, 3/12/1998–4/16/1998, 20 values) and (c, d) *ROMEO* buoy (36°N, 75°W, 10/22/1999–11/30/1999, 35 values).

Table 4. Bias, RMSD and r for LHF, SHF and Pertinent Variables Calculated in Comparisons Between Daily Buoy Data From *FETCH* and *ROMEO* and IFREMER, WHOI OAFlux[a]

	FETCH						*ROMEO*					
Variable	IF B	W B	IF R	W R	IF r	W r	IF B	W B	IF R	W R	IF r	W r
LHF (W m^{-2})	−9.1	−3.5	34.8	21.6	0.8	0.9	33.1	59.0	81.7	10.0	0.8	0.9
SHF (W m^{-2})	9.7	−0.5	20.4	9.6	0.7	0.8	−19.4	27.9	47.2	36.9	0.2	0.9
SST (°C)	−0.1	−0.3	0.4	0.4	0.7	0.6	3.3	3.1	3.6	3.3	0.5	0.7
Q_a (g kg^{-1})	0.5	−0.6	1.0	0.8	0.8	1.0	−1.9	0.0	2.7	0.8	0.9	1.0
U (m s^{-1})	0.8	−0.7	2.5	1.4	0.7	0.9	1.9	0.2	2.6	1.7	0.9	0.9
T_a (°C)	−0.4	−0.1	1.3	0.7	0.7	0.9	4.2	0.4	5.1	1.0	0.1	1.0

[a]Bias (B), RMSD (R),IFREMER (IF) and WHOI OAFlux (W).

Any uncertainties in wind speed measurements could be due to difficulties in measuring by satellite the strong Mistral and Tramontane winds, which are northerly northwesterly winds produced by the synoptic regime and topography of the south of France, north of Italy, and northwest of Spain, found in the experiment area during that time [*Hauser et al.*, 2003]. Also, *Drennan et al.* [2003] mentioned the importance of swell conditions on the behavior of the wave boundary layer and that the presence of swell waves cannot be scaled based on the Monin-Obukhov theory. Swells can modify and increase the scatter of the drag coefficient relations compared to the pure wind sea regime. Negatively biased WHOI OAFlux sea surface temperature values compared to those from the *FETCH* buoy (−0.3°C) could explain their sensible heat flux bias; this is confirmed by Q_{T_s} contributing the most to the total of the Q terms for WHOI-*FETCH* sensible heat flux (−1.9 W m^{-2}).

4.2.3. Comparison to *ROMEO* Buoy

[45] The independent *ROMEO* buoy is located near the Gulf Stream, an area of large differences between the two data sets as indicated in section 4.1; comparison of flux estimates to the values from experiment is important for the examination of uncertainties. Also note that this area is close to a very strong SST gradient. The RMSD of latent heat flux between IFREMER and *ROMEO* is over 80 W m^{-2}, which is not surprising since specific surface humidity is a function of SST, which satellites may not be able to measure as accurately in areas of high SST gradient [*Reynolds et al.*, 2007]. According to Figure 5 and Table 4, IFREMER latent heat fluxes exhibit a positive bias compared to *ROMEO* latent heat fluxes of 33.1 Wm^{-2}, but sensible heat fluxes are biased by −19.4 W m^{-2}; the WHOI OAFlux latent and sensible heat flux biases were both positive and greater in magnitude than those of IFREMER, 59.0 and 27.9 W m^{-2} respectively.

[46] Using the Q term analysis for IFREMER-*ROMEO* data, a positive observationally averaged Q_{Q_S} is nearly balanced by a negative Q_{Q_A}, but Q_{U_A} is 26.8 W m^{-2}, which contributes to a positive total Q term for latent heat flux (Table 5); this makes sense based on the positive bias exhibited by IFREMER wind speed compared to *ROMEO* data. The major contributor to the total Q term for IFREMER-*ROMEO* sensible heat flux is Q_{T_A}, which corresponds to a large positive bias in IFREMER air temperature of 4.2°C. Q_{T_S} also contributed significantly to IFREMER sensible heat flux uncertainty (31.7 W m^{-2}). This large difference in air humidity and temperature over the Gulf Stream are due in part to the periodic presence of cold, dry continental air over the region. *Grodsky et al.* [2009] performed a regression analysis that suggested correspondence between the strengthening of intraseasonal latent heat flux in the Gulf Stream region and midlatitude storm systems in the Atlantic. Increases in latent heat flux in this region correspond to an area of low sea level pressure and cyclonic anomalous winds center east of the region; this anomalous wind decelerates the northern flank of the northeasterly trade winds, and accelerates offshore flow over the Gulf Stream. The atmospheric boundary layer adjustment [*Beal et al.*, 1997] adds to the acceleration over the warm sector of the Gulf Stream. In addition to wind intensification, the northwesterly wind outbreaks bring cold and dry continental air over the sea as mentioned before, lowering air humidity, and increasing the air-sea moisture gradient. Also, note that satellite algorithms for humidity and air temperature over the ocean are tuned to maritime air masses, and clearly have problems in these regions. This is discussed further below.

[47] For WHOI-*ROMEO*, Q_{Q_S} contributed the most to the total Q term for latent heat flux, since WHOI OAFlux sea surface temperature was positively biased compared to ground truth; for WHOI OAFlux sensible heat fluxes, Q_{T_S} (29.5 W m^{-2}) contributed most to the total of the Q terms for WHOI-*ROMEO* sensible heat flux.

4.2.4. Test of an Alternate Method for Near Surface Specific Humidity and Air Temperature

[48] When comparing to data from *FETCH* and *ROMEO*, the Q term analysis showed that specific air humidity contributed the most to the bias of IFREMER latent heat fluxes, and air temperature contributed the most to the IFREMER sensible heat flux bias. For estimates of specific air humidity, both data sets used algorithms that were a function of other variables. Satellite brightness temperature from SSM/I were

Table 5. The Average of the Q Terms for *FETCH* and *ROMEO* Observations Versus IFREMER and WHOI OAFlux[a]

	FETCH		*ROMEO*	
Q Term	IF	W	IF	W
Q_{C_E}	0.6	−0.4	1.7	−0.3
Q_{U_A}	6.6	−9.7	26.8	−8.7
Q_{Q_S}	−1.4	6.6	55.6	81.1
Q_{Q_A}	−15.9	0.9	−55.2	−14.8
Q_{Total}	−10.1	−2.6	28.9	57.3
dL_E	−9.1	−3.5	33.1	59.0
Q_{C_H}	0.1	−0.0	0.4	−0.1
Q_{U_A}	1.9	−1.0	3.0	−3.7
Q_{T_S}	−0.6	−1.9	31.7	29.5
Q_{T_A}	7.7	1.5	−48.5	−4.6
Q_{Total}	9.1	−1.4	−13.4	21.1
dL_H	9.7	−0.5	−19.4	27.9

[a]IF, IFREMER (IF); W, WHOI OAFlux. Units are W m^{-2}.

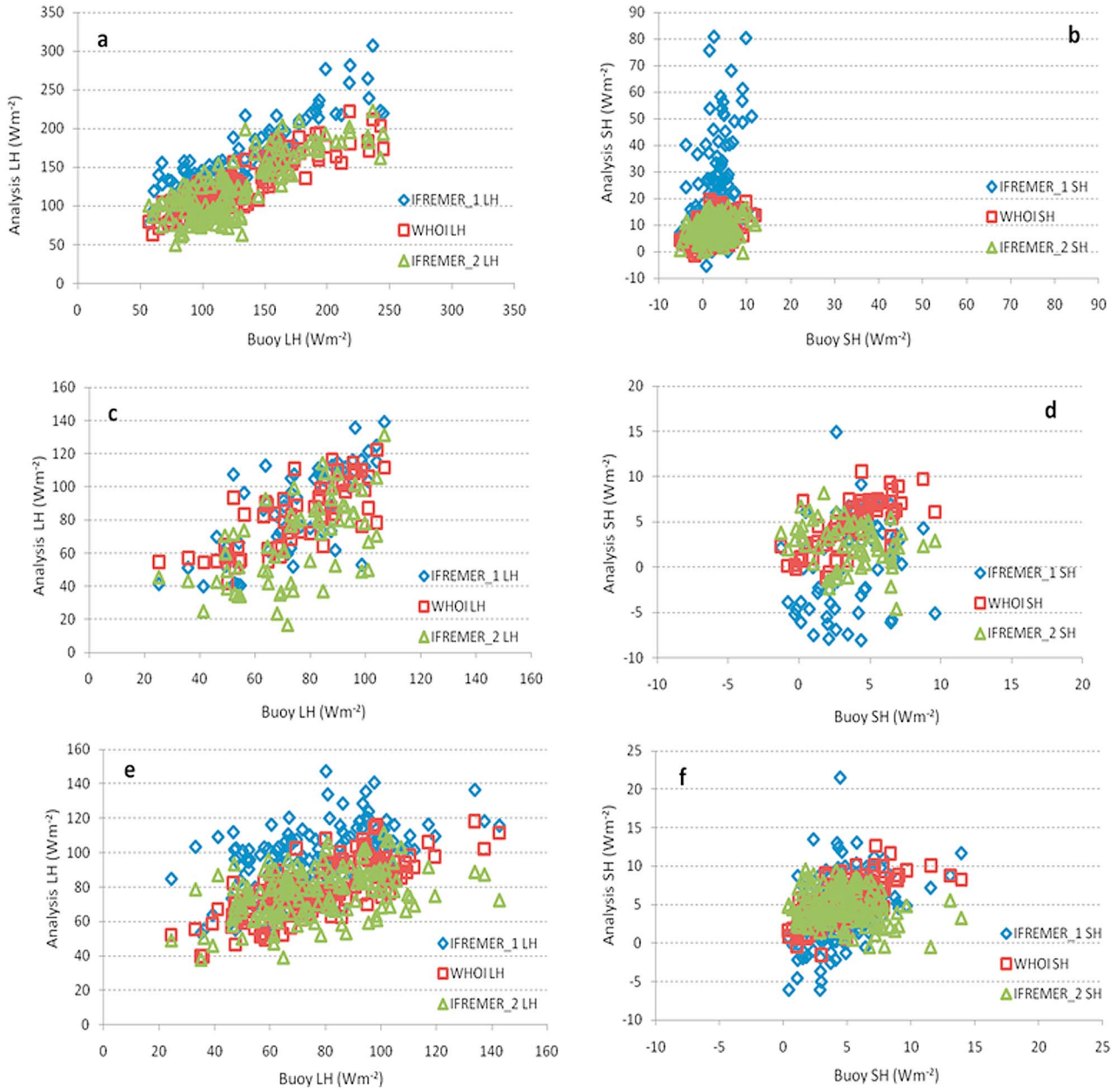

Figure 6. Comparison of weekly averaged buoy latent (LH) and sensible heat flux (SH) to IFREMER_1, WHOI OAFlux and IFREMER_2 (IFREMER_1 SST and 10 m wind speed and *Jackson et al.* [2009] 10 m specific air humidity and air temperature) estimates at three *PIRATA* buoy locations: (a, b) 15°N, 38°W (1/26/1998–12/26/2005, 136 values), (c, d) 0°N, 10°W (9/15/1997–12/26/2005, 63 values) and (e, f) 0°N, 23°W (3/1/1999–12/26/2005, 148 values).

used for the IFREMER estimate, and precipitable water measurements from SSM/I were used for the WHOI OAFlux estimate. However, WHOI also used values for specific air humidity from ERA-40 and NCEP re-analyses. IFREMER calculated air temperature indirectly using the Bowen Ratio method of *Konda et al.* [1996] that depends on sea surface temperature, surface wind speed and specific air humidity. Any biases in input variables are inherently included in calculating air temperature.

[49] Use of other methods to calculate specific air humidity and air temperature from satellites could aid in more accurate estimates of these variables, and, in turn, in estimates of heat fluxes. For example, *Jackson et al.* [2006, 2009] derived satellite-based estimates of specific air humidity and air temperature by combining ship, buoy and satellite microwave observations from the Advanced Microwave Sounding Unit (AMSU-A), Special Sensor Microwave Temperature Sounder (SSM/T-2) and SSM/I based on multiple linear regressions. A multisensor approach using microwave sounders can improve the retrieval of these two variables by incorporating additional information about the tropospheric humidity and temperature profiles.

Table 6. Bias, RMSD and r for Comparison of Weekly-Averaged Latent and Sensible Heat Fluxes to IFREMER_1, WHOI OAFlux and IFREMER_2[a]

Data	LH B	LH R	LH r	SH B	SH R	SH r
			PIRATA (15°N, 38°W)			
IF_1	24.3	34.0	0.9	18.6	24.9	0.4
W	−3.2	20.4	0.9	5.0	6.4	0.5
IF_2	−4.1	26.8	0.8	6.0	7.4	0.2
			PIRATA (0°N, 10°W)			
IF_1	11.8	21.4	0.7	−3.2	6.0	0.3
W	7.2	15.2	0.8	0.9	2.2	0.7
IF_2	−7.8	22.3	0.6	−1.1	4.0	−0.2
			PIRATA (0°N, 23°W)			
IF_1	20.4	28.2	0.5	−0.1	4.0	0.4
W	2.0	14.6	0.8	0.6	2.1	0.7
IF_2	0.2	20.7	0.4	0.2	3.6	−0.2
			ROMEO (36°N, 75°W)			
IF_1	21.9	89.8	0.8	−38.3	65.1	0.0
W	61.0	83.8	0.9	34.0	44.6	0.9
IF_2	61.2	98.6	0.8	−20.1	44.7	0.8

[a]Bias (B), RMSD (R), latent and sensible heat flux (LH and SH), IFREMER_1 (IF_1), WHOI OAFlux (W) and IFREMER_2 (IF_2). IFREMER_1 SST and 10 m wind speed and *Jackson et al.* [2009] 10 m specific air humidity and air temperature. Estimates at three *PIRATA* buoy locations, 15°N, 38°W (1/26/1998–12/26/2005, 136 values), 0°N, 10°W (9/15/1997–12/26/2005, 63 values) and 0°N, 23°W (3/1/1999–12/26/2005, 148 values), and at the *ROMEO* buoy location (36°N, 75°W, 10/22/1999–11/30/1999, 14 values). Units are W m^{-2}.

[50] As an initial test, we use the SST and 10 m wind speed provided by IFREMER and the 10 m specific humidity and temperature from *Jackson et al.* [2009] (courtesy of G. Wick) as input variables into the COARE3.0 algorithm and estimate latent and sensible heat fluxes at three *PIRATA* buoy locations, 15°N, 38°W, 0°N, 10°W and 0°N, 23°W, and at the *ROMEO* buoy location, 36°N, 75°W; these buoys are in areas where fluxes showed the largest discrepancies. The new turbulent flux estimates at these locations (known as IFREMER_2) were compared to ground truth at these locations. As seen in Figures 6a–6d and Table 6, when compared to the *PIRATA* fluxes, at the 15°N, 38°W and 0°N, 10°W buoys, the IFREMER_2 latent and sensible heat flux estimates are significantly improved over that of IFREMER_1 (the original IFREMER estimate) in terms of weekly averaged bias. As for 0°N, 23°W, the IFREMER_2 latent heat flux estimate are an improvement over WHOI OAFlux, and the IFREMER_2 sensible heat flux bias is lower than that of IFREMER_1 (Figures 6e and 6f and Table 6). At the *ROMEO* buoy location, IFREMER_1 actually gives the best latent heat flux estimate, but IFREMER_2 sensible heat flux is superior to those of IFREMER_1 and WHOI OAFlux (Figure 7 and Table 6). Thus, use of the *Jackson et al.* data and methods can further improve latent and sensible heat flux estimates that are satellite-based, but other modifications in choice of sea surface temperature and wind speed products as well as different implementation of the COARE algorithm need to be considered.

5. Conclusions

[51] Examination of two estimates of annual means of latent and sensible heat fluxes during 1996–2005, from IFREMER and from WHOI OAFlux over the Atlantic basin (70°W–30°E, 45°S–45°N), showed that IFREMER fluxes were larger in most regions with the exception of some small areas off the West African coast, the Gulf Stream region and south of 30°S; this coincides with IFREMER's lower specific air humidity and air temperature values in almost all regions of the Atlantic with the same exceptions as stated above. When compared to the *FETCH* and *ROMEO* buoys, the Q term analysis showed that specific air humidity contributed the most to the total difference between IFREMER and buoy latent heat fluxes, and that the Q term corresponding to air temperature was the largest of the Q terms for IFREMER-buoy sensible heat fluxes.

[52] Another possible explanation is the inability of satellites to account for certain meteorological and oceanographic conditions, such as low level stratus clouds over cold water [*Smith et al.*, 2010]. There were high wind speeds as well as a dramatic drop in air temperatures during the period of the deployment of *ROMEO* due to the passage of a cold front [*Zhang et al.*, 2009]. It is known that satellites have difficulty capturing effects of atmospheric stratification, when there are cold air outbreaks over the ocean as well as high wind speeds [*Bentamy et al.*, 2003]. Thus, in both experiments, uncertainty in satellite estimates compared to ground truth could be

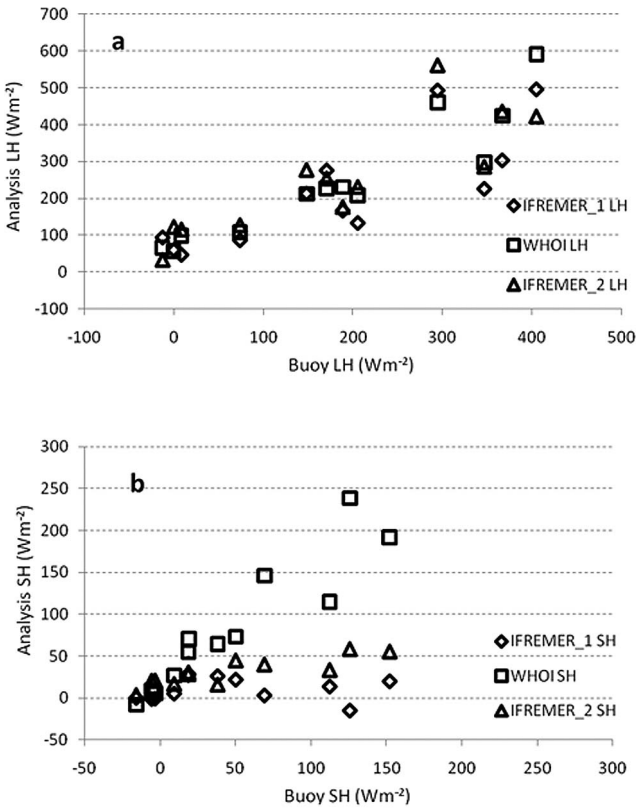

Figure 7. Comparison of daily averaged (a) buoy latent (LH) and (b) sensible heat flux (SH) to IFREMER_1, WHOI OAFlux and IFREMER_2 (IFREMER_1 SST and 10 m wind speed and *Jackson et al.* [2009] 10 m specific air humidity and air temperature) estimates at the *ROMEO* buoy location (36°N, 75°W, 10/22/1999–11/30/1999, 14 values).

attributed to these impacts by the weather regimes, showing a need to improve interpolation in time and space in order for satellite estimates to better reflect conditions during synoptic-scale storms and fronts.

[53] In addition, coastal upwelling present off the West African coast could affect satellite estimates of fluxes, as was seen in the spatial analysis of the differences between IFREMER and WHOI OAFlux in section 4.1. In cold tongue regions, the mixed layer temperature balance is dominated by not only upwelling but also tropical instability waves that horizontally transport heat [*Grodsky et al.*, 2009]. Again, due to the impact of upwelling on stratification, satellites may not be able to identify effects on near surface humidity, air temperature and air-sea fluxes in such areas. The effect of limited input data on numerical analyses in the Southern Hemisphere may also affect the underlying model fluxes in the case of WHOI OAFlux estimates. There is no way to know without good in situ comparison data which estimate is better when they differ in systematic ways. Strong storm systems that propagate over the Agulhas Current region off the South African coast produce strong latent heat flux; depending on the location of the storm center, this heat flux is sometimes amplified by anomalous southerly winds that bring dry and cold sub-Antarctic air northward [*Grodsky et al.*, 2009]. The satellite observations may be unable to handle this phenomenon properly, which could cause a discrepancy between IFREMER and WHOI OAFlux products in this region. Model fluxes may also suffer here where there is little in situ data to assimilate into the WHOI OAFlux product.

[54] Finally, conditions in the Gulf Stream region present similar challenges in satellite flux estimation, including strong surface currents and SST gradients as well as how the stratified atmospheric boundary layer amplifies air-sea interactions on an intraseasonal timescale [*Grodsky et al.*, 2009]. The fact that IFREMER used the *Reynolds et al.* [2007] product that included AMSR-E data merged with AVHRR data from 2002 on compared to WHOI's use of the AVHRR-only data may have been part of the reason for larger discrepancies in their SST estimates. It may well be that there are systematic differences between the two products due to the sampling, which leads to three conclusions: (1) the merged product (i.e., IFREMER) is better post-2002 due to AMSR and AVHRR merged SST data improving spatial resolution of SST gradient features [*Reynolds et al.*, 2007], (2) the discontinuity in 2002 is an artifact and (3) both AVHRR-only products have larger total error (random plus sampling plus bias [see *Reynolds et al.*, 2007]). Some consideration of the limitations of each method in the Gulf Stream and other areas of variable SST and cold air outbreaks may be possible with modern statistical methods. In the past, regionally varied empirical formulas have been avoided due to artificial boundaries in the resulting products, but the time may now be right for including existing knowledge of regional and seasonal patterns when generating these types of products, especially since the supporting information for making the algorithm choices may be available from NWP models or supplemental satellite observations.

[55] *Curry et al.* [2004] state that a combination of satellite and reanalysis data currently yields the most accurate representation of air-sea fluxes, but WHOI OAFlux being dependent on numerical models to a larger extent may have limitations in certain specialized circumstances. For example, humidity data from radiosondes are known to exhibit dry and wet biases, which depend on the radiosondes' type and age as well as the conditions of the environment [*Wang et al.*, 2002]. Since radiosonde data are assimilated into numerical models, their biases can impact NWP model analyses and subsequent forecasts; *Bock et al.* [2007] showed that, for measurements of precipitable water vapor (PWV), which can be used to estimate humidity, over Africa (35°N–10°S), there were dry biases of 12–14% in radiosonde data compared to Global Positioning System (GPS) data, which partially explain biases of up to 9% for ERA-40 PWV data and up to 14% for NCEP2 PWV data.

[56] Use of satellite data to estimate turbulent air-sea heat fluxes could be considered optimal due to the global coverage and high resolution provided by satellites. Satellite-derived fluxes have been shown to be an improvement over NWP fluxes, especially in tropical regions [*Yu et al.*, 2004; *Mestas-Nuñez et al.*, 2006]. In addition, *Ayina et al.* [2006] reported that the forcing of an ocean circulation model with satellite fluxes instead of NWP fluxes improves calculations of currents and SST compared to tropical buoy data. Areas in need of improvement in regard to input of data, methodology and geographical location have been cited here. In addition, an attempt at improvement has been made using the data of *Jackson et al.* [2009]. In the future, we will also consider the inconsistency of calibration of certain SSM/I products as well as the change in how QuikSCAT winds were estimated after the implementation of a new geophysical model from the Jet Propulsion Laboratory in 2006 relating wind to backscatter. A careful and rigorous effort to address these concerns and comprehensively test new approaches and data sources is required in order to achieve the goal of an accuracy of 5 W m^{-2} set by the Global Energy and Water Cycle Experiment Radiation Panel and the United States Climate Variability and Predictability Committee [*Curry et al.*, 2004]. Continued effort will eventually ensure that such a data set is produced which allows examination of climate phenomena and realistic studies on the net air-sea heat fluxes and the budgets of heat as well as salinity in the upper ocean.

Appendix A: *Bourras*'s [2006] Q Term Method

[57] The bulk parameterizations of latent and sensible heat fluxes, L_E and L_H, (written as LHF and SHF in the main text) are given as

$$L_E = \rho L_V C_E U_A (Q_S - Q_A) \tag{A1}$$

$$L_H = \rho C_p C_H U_A (T_S - T_A) \tag{A2}$$

where ρ is air density, L_V is the latent heat of vaporization, C_p is the specific heat capacity of air at constant pressure, and Q_A, T_A, and U_A are specific humidity, air temperature and wind speed at a specified height above the surface. Q_S and T_S are the specific humidity and temperature at the sea surface; Q_S is assumed to be 98% of the saturation humidity at the sea surface temperature. C_E and C_H are moisture and

heat exchange coefficients. Differentiating (A1) and (A2) result in

$$dL_E = \left(\frac{\partial L_E}{\partial C_E}\right) dC_E + \left(\frac{\partial L_E}{\partial U_A}\right) dU_A + \left(\frac{\partial L_E}{\partial Q_A}\right) dQ_A + \left(\frac{\partial L_E}{\partial Q_S}\right) dQ_S \tag{A3}$$

$$dL_H = \left(\frac{\partial L_H}{\partial C_H}\right) dC_H + \left(\frac{\partial L_H}{\partial U_A}\right) dU_A + \left(\frac{\partial L_H}{\partial T_A}\right) dT_A + \left(\frac{\partial L_H}{\partial T_S}\right) dT_S \tag{A4}$$

where

$$\begin{aligned}
\frac{\partial L_E}{\partial C_E} &= \rho L_V U_A (Q_S - Q_A) \\
\frac{\partial L_E}{\partial U_A} &= \rho L_V C_E (Q_S - Q_A) \\
\frac{\partial L_E}{\partial Q_S} &= \rho L_V C_E U_A \\
\frac{\partial L_E}{\partial Q_A} &= -\rho L_V C_E U_A \\
\frac{\partial L_H}{\partial C_H} &= \rho C_p U_A (T_S - T_A) \\
\frac{\partial L_H}{\partial U_A} &= \rho C_p C_H (T_S - T_A) \\
\frac{\partial L_H}{\partial T_S} &= \rho C_p C_H U_A \\
\frac{\partial L_H}{\partial T_A} &= -\rho C_p C_H U_A
\end{aligned} \tag{A5}$$

and

$$\begin{aligned}
dL_E &= L_E(estimated) - L_E(buoy) \\
dC_E &= C_E(estimated) - C_E(buoy) \\
dU_A &= U_A(estimated) - U_A(buoy) \\
dQ_A &= Q_A(estimated) - Q_A(buoy) \\
dQ_S &= Q_S(estimated) - Q_S(buoy) \ . \\
dL_H &= L_H(estimated) - L_H(buoy) \\
dC_H &= C_H(estimated) - C_H(buoy) \\
dT_A &= T_A(estimated) - T_A(buoy) \\
dT_S &= T_S(estimated) - T_S(buoy)
\end{aligned} \tag{A6}$$

[58] Combining (A2), (A3) and (A4), dL_E and dL_H can be rewritten as

$$\begin{aligned}
dL_E &= Q_{C_E} + Q_{U_A} + Q_{Q_A} + Q_{Q_S} = Q_{tot} \\
dL_H &= Q_{C_H} + Q_{U_A} + Q_{T_A} + Q_{T_S} = Q_{tot}
\end{aligned} \tag{A7}$$

where the "Q terms" are the contributions to the deviation between estimated and buoy fluxes.

[59] **Acknowledgments.** We thank NSF for support under grants ATM0631685 to the University of Maryland, ATM0631792 to the University of Miami, and ATM0631677 to Texas A&M University-Corpus Christi. The work also benefited from support under NASA grant NNG05GB35G to the University of Maryland. We thank the anonymous reviewers for their helpful comments.

References

Ayina, L.-H., A. Bentamy, A. M. Mestas-Nuñez, and G. Madec (2006), The impact of satellite winds and latent heat fluxes in a numerical simulation of the tropical Pacific Ocean, *J. Clim.*, *19*, 5889–5902, doi:10.1175/JCLI3939.1.

Beal, R. C., V. N. Kudryavtsev, D. R. Thompson, S. A. Grodsky, D. G. Tilley, V. A. Dulov, and H. C. Graber (1997), The influence of the marine atmospheric boundary layer on ERS 1 synthetic aperture radar imagery of the Gulf Stream, *J. Geophys. Res.*, *102*, 5799–5814, doi:10.1029/96JC03109.

Beljaars, A. C. M. (1995a), The impact of some aspects of the boundary layer scheme in the ECMWF model, paper presented at Seminar on Parameterization of Sub-Grid Scale Physical Processes, Eur. Cent. for Medium-Range Weather Forecasts, Reading, U. K.

Beljaars, A. C. M. (1995b), The parameterization of surface fluxes in large scale models under free convection, *Q. J. R. Meteorol. Soc.*, *121*, 255–270, doi:10.1002/qj.49712152203.

Beljaars, A., and P. Kallberg (2001), Ocean fluxes in the ECMWF 40-year re-analysis (ERA40), paper presented at Workshop on Intercomparison and Validation of Ocean-Atmosphere Flux Fields, World Clim. Res. Program, Washington, D. C.

Bentamy, A., P. Queffeulou, Y. Quilfen, and K. Katsaros (1999), Ocean surface wind fields estimated from satellite active and passive microwave instruments, *IEEE Trans. Geosci. Remote Sens.*, *37*, 2469–2486, doi:10.1109/36.789643.

Bentamy, A., K. B. Katsaros, A. M. Mestas-Nuñez, W. M. Drennan, E. B. Forde, and H. Roquet (2003), Satellite estimates of wind speed and latent heat flux over the global oceans, *J. Clim.*, *16*, 637–656, doi:10.1175/1520-0442(2003)016<0637:SEOWSA>2.0.CO;2.

Bentamy, A., L.-H. Ayina, W. Drennan, K. Katsaros, A. M. Mestas-Nuñez, and R. T. Pinker (2008), 15 years of ocean surface momentum and heat fluxes from remotely sensed observations, *FLUXNEWS*, *5*, 14–16. [Available at http://sail.msk.ru/newsletter/fluxnews_5_final.pdf.]

Berrisford, P., D. Dee, K. Fielding, M. Fuentes, P. Källberg, S. Kobayashi, and S. Uppala (2009), The ERA-interim archive, version 1.0, report, Eur. Cent. for Medium Range Weather Forecasts, Reading, UK.

Bock, O., M.-N. Bouin, A. Walpersdorf, J.-P. Lafore, S. Janicot, F. Guichard, and A. Agusti-Panareda (2007), Comparison of ground-based GPS precipitable water vapour to independent observations and numerical weather prediction model reanalyses over Africa, *Q. J. R. Meteorol. Soc.*, *133*, 2011–2027, doi:10.1002/qj.185.

Bourras, D. (2006), Comparison of five satellite-derived latent heat flux products to moored buoy data, *J. Clim.*, *19*, 6291–6313, doi:10.1175/JCLI3977.1.

Bourras, D., L. Eymard, and W. T. Liu (2002), A neural network to estimate the latent heat flux over oceans from satellite observations, *Int. J. Remote Sens.*, *23*, 2405–2423, doi:10.1080/01431160110070825.

Brunke, M. A., X. Zeng, and S. Anderson (2002), Uncertainties in sea surface turbulent flux algorithms and data sets, *J. Geophys. Res.*, *107*(C10), 3141, doi:10.1029/2001JC000992.

Brunke, M. A., C. W. Fairall, X. Zeng, L. Eymard, and J. A. Curry (2003), Which bulk aerodynamic algorithms are least problematic in computing ocean surface turbulent fluxes?, *J. Clim.*, *16*, 619–635, doi:10.1175/1520-0442(2003)016<0619:WBAAAL>2.0.CO;2.

Cavalieri, D. J., C. L. Parkinson, P. Gloersen, J. C. Comiso, and H. J. Zwally (1999), Deriving long-term time series of sea ice cover from satellite passive-microwave multisensor data sets, *J. Geophys. Res.*, *104*(C7), 15,803–15,814, doi:10.1029/1999JC900081.

Cayan, D. R. (1992), Latent and sensible heat flux anomalies over the northern oceans: Driving the sea surface temperature, *J. Phys. Oceanogr.*, *22*, 859–881, doi:10.1175/1520-0485(1992)022<0859:LASHFA>2.0.CO;2.

Chang, H.-R., and R. L. Grossman (1999), Evaluation of bulk surface flux algorithms for light wind conditions using data from the Coupled Ocean-Atmosphere Response Experiment (COARE), *Q. J. R. Meteorol. Soc.*, *125*, 1551–1588, doi:10.1002/qj.49712555705.

Chou, S.-H. (1993), A comparison of airborne eddy correlation and bulk aerodynamic methods for ocean-air turbulent fluxes during cold-air outbreaks, *Boundary Layer Meteorol.*, *64*, 75–100, doi:10.1007/BF00705663.

Chou, S.-H., R. Atlas, C.-L. Shie, and J. Ardizzone (1995), Estimates of surface humidity and latent heat fluxes over oceans from SSM/I data, *Mon. Weather Rev.*, *123*, 2405–2425, doi:10.1175/1520-0493(1995)123<2405:EOSHAL>2.0.CO;2.

Chou, S.-H., C.-L. Shie, R. M. Atlas, and J. Ardizzone (1997), Air-sea fluxes retrieved from Special Sensor Microwave Imager data, *J. Geophys. Res.*, *102*, 12,706–12,726, doi:10.1029/97JC00978.

Chou, S.-H., E. Nelkin, J. Ardizzone, R. M. Atlas, and C.-L. Shie (2003), Surface turbulent heat and momentum fluxes over global oceans based on the Goddard Satellite Retrievals, Version 2(GSSTF2), *J. Clim.*, *16*, 3256–3273, doi:10.1175/1520-0442(2003)016<3256:STHAMF>2.0.CO;2.

Chou, S.-H., E. Nelkin, J. Ardizzone, and R. M. Atlas (2004), A comparison of latent heat fluxes over global oceans for four flux products, *J. Clim.*, *17*, 3973–3989, doi:10.1175/1520-0442(2004)017<3973:ACOLHF>2.0.CO;2.

Cione, J. J., and E. W. Uhlhorn (2003), Sea surface temperature variability in hurricanes: Implications with respect to intensity change, *Mon. Weather Rev.*, *131*, 1783–1796, doi:10.1175//2562.1.

Curry, J. A., et al. (2004), SEAFLUX, *Bull. Am. Meteorol. Soc.*, *85*, 409–424, doi:10.1175/BAMS-85-3-409.

da Silva, A., A. C. Young, and S. Levitus (1994), *Atlas of Surface Marine Data 1994*, vol. 1, *Algorithms and Procedures*, *NOAA Atlas NESDIS*, vol. 6, 83 pp., NOAA, Silver Spring, Md.

Drennan, W. M., H. C. Graber, D. Hauser, and C. Quentin (2003), On the wave age dependence of wind stress over pure wind seas, *J. Geophys. Res.*, *108*(C3), 8062, doi:10.1029/2000JC000715.

Fairall, C. W., E. F. Bradley, D. P. Rogers, J. B. Edson, and G. S. Young (1996), Bulk parameterization of air-sea fluxes for Tropical Ocean-Global Atmosphere Coupled-Ocean Atmosphere Response Experiment, *J. Geophys. Res.*, *101*, 3747–3764, doi:10.1029/95JC03205.

Fairall, C. W., E. F. Bradley, J. E. Hare, A. A. Grachev, and J. B. Edson (2003), Bulk parameterization of air-sea fluxes: Updates and verification for the COARE3.0 algorithm, *J. Clim.*, *16*, 571–591, doi:10.1175/1520-0442(2003)016<0571:BPOASF>2.0.CO;2.

Fennig, K., S. Bakan, H. Grassl, C.-P. Klepp, and J. Schulz (2006), Hamburg Ocean Atmosphere Parameters and Fluxes from Satellite Data - HOAPS II - Monthly Mean, http://cera-www.dkrz.de/WDCC/ui/Compact.jsp?acronym=HOAPS2_MONTHLY, World Data Cent. for Clim., Hamburg, Germany.

Gibson, J. K., P. Kallberg, S. Uppala, A. Hernandez, A. Nomura, and E. Serrano (1997), ECMWF reanalysis project report series. Part I. ERA description, report, 72 pp., Eur. Cent. for Medium Range Weather Forecasts, Reading, U. K.

Graber, H. C., E. A. Terray, M. A. Donelan, W. M. Drennan, J. C. Van Leer, and D. B. Peters (2000), ASIS—A new air–sea interaction spar buoy: Design and performance at sea, *J. Atmos. Oceanic Technol.*, *17*, 708–720, doi:10.1175/1520-0426(2000)017<0708:AANASI>2.0.CO;2.

Grassl, H., V. Jost, R. Kumar, J. Schulz, P. Bauer, and P. Schussel (2000), The Hamburg Ocean-Atmosphere Parameters and Fluxes from Satellite Data (HOAPS): A climatological atlas of satellite-derived air-sea interaction parameters over the oceans, *Rep. 312*, Max Planck Inst. for Meteorol., Hamburg, Germany.

Grodsky, S. A., A. Bentamy, J. A. Carton, and R. T. Pinker (2009), Intraseasonal latent heat flux based on satellite observations, *J. Clim.*, *22*, 4539–4556, doi:10.1175/2009JCLI2901.1.

Grumbine, R. W. (1996), Automated passive microwave sea ice concentration analysis at NCEP, report, Environ. Model. Cent., Camp Springs, Md. [Available at http://polar.ncep.noaa.gov/seaice/docs/ssmi.auto/ssmi120.shtml.]

Hauser, D., et al. (2003), The FETCH experiment: An overview, *J. Geophys. Res.*, *108*(C3), 8053, doi:10.1029/2001JC001202.

Houghton, R. W. (1991), The relationship of sea surface temperature to thermocline depth at annual and interannual time scales in the tropical Atlantic Ocean, *J. Geophys. Res.*, *96*(C8), 15,173–15,185, doi:10.1029/91JC01442.

Jackson, D. L., G. A. Wick, and J. J. Bates (2006), Near-surface retrieval of air temperature and specific humidity using multisensory microwave satellite observations, *J. Geophys. Res.*, *111*, D10306, doi:10.1029/2005JD006431.

Jackson, D. L., G. A. Wick, and F. R. Robertson (2009), Improved multisensor approach to satellite-retrieved near-surface specific humidity observations, *J. Geophys. Res.*, *114*, D16303, doi:10.1029/2008JD011341.

Jones, C., P. Peterson, and C. Gautier (1999), A new method for deriving ocean surface specific humidity and air temperature: An artificial neural network approach, *J. Appl. Meteorol.*, *38*, 1229–1245, doi:10.1175/1520-0450(1999)038<1229:ANMFDO>2.0.CO;2.

Josey, S. A. (2001), A comparison of ECMWF, NCEP-NCAR AND SOC surface heat fluxes with moored buoy measurements in the subduction region of the northeast Atlantic, *J. Clim.*, *14*, 1780–1789, doi:10.1175/1520-0442(2001)014<1780:ACOENN>2.0.CO;2.

Kalnay, E., et al. (1996), The NCEP/NCAR 40-year reanalysis project, *Bull. Am. Meteorol. Soc.*, *77*, 437–471, doi:10.1175/1520-0477(1996)077<0437:TNYRP>2.0.CO;2.

Kistler, R., et al. (2001), The NCEP-NCAR 50-year reanalysis: Monthly means CD-ROM and documentation, *Bull. Am. Meteorol. Soc.*, *82*(2), 247–267, doi:10.1175/1520-0477(2001)082<0247:TNNYRM>2.3.CO;2.

Konda, M., N. Imasato, and A. Shibata (1996), A new method to determine near-sea surface air temperature by using satellite data, *J. Geophys. Res.*, *101*, 14,349–14,360, doi:10.1029/96JC00796.

Kubota, M., N. Iwasaka, S. Kizu, M. Kondo, and K. Kutsuwada (2002), Japanese ocean flux data sets with use of remote sensing observations (J-OFURO), *J. Oceanogr.*, *58*, 213–225, doi:10.1023/A:1015845321836.

Kubota, M., A. Kano, H. Muramatsu, and H. Tomita (2003), Intercomparison of various surface latent heat flux fields, *J. Clim.*, *16*, 670–678, doi:10.1175/1520-0442(2003)016<0670:IOVSLH>2.0.CO;2.

McPhaden, M. J., et al. (1998), The Tropical Ocean-Global Atmosphere (TOGA) observing system: A decade of progress, *J. Geophys. Res.*, *103*, 14,169–14,240, doi:10.1029/97JC02906.

McPhaden, M. J., Y. Kuroda, and V. S. N. Murty (2006), Development of an Indian Ocean moored buoy array for climate studies, *CLIVAR Exch.*, *11*(4), 3–5.

Mestas-Nuñez, A. M., and D. B. Enfield (1999), Rotated global modes of non-ENSO sea surface temperature variability, *J. Clim.*, *12*, 2734–2746, doi:10.1175/1520-0442(1999)012<2734:RGMONE>2.0.CO;2.

Mestas-Nuñez, A. M., A. Bentamy, and K. B. Katsaros (2006), Seasonal and El Niño variability in weekly satellite evaporation over the global ocean during 1996–98, *J. Clim.*, *19*, 2025–2035, doi:10.1175/JCLI3721.1.

Moyer, K. A., and R. A. Weller (1997), Observations of surface forcing from the subduction experiment: A comparison with global model products and climatological data sets, *J. Clim.*, *10*, 2725–2742, doi:10.1175/1520-0442(1997)010<2725:OOSFFT>2.0.CO;2.

Navarra, A., W. F. Stern, and K. Miyakoda (1994), Reduction of the Gibbs oscillation in spectral model simulations, *J. Clim.*, *7*, 1169–1183, doi:10.1175/1520-0442(1994)007<1169:ROTGOI>2.0.CO;2.

Niiler, P. P., and E. B. Kraus (1977), One-dimensional models of the upper ocean, in *Modelling and Prediction of the Upper Layers of the Ocean*, edited by E. B. Kraus, pp. 143–172, Pergamon, Oxford, U. K.

Oost, W. A., G. J. Komen, C. M. J. Jacobsm, and C. van Oort (2002), New evidence for a relation between wind stress and wave age from measurements during ASGAMAGE, *Boundary Layer Meteorol.*, *103*, 409–438, doi:10.1023/A:1014913624535.

Reynolds, R. W., T. M. Smith, C. Liu, D. B. Chelton, K. S. Casey, and M. G. Schlax (2007), Daily high-resolution-blended analyses for sea surface temperature, *J. Clim.*, *20*, 5473–5496, doi:10.1175/2007JCLI1824.1.

Schulz, J., P. Schlussel, and H. Grassl (1993), Water vapor in the atmospheric boundary layer over oceans from SSM/I measurements, *Int. J. Remote Sens.*, *14*, 2773–2789, doi:10.1080/01431169308904308.

Schulz, J., J. Meywerk, S. Ewald, and P. Schlüssel (1997), Evaluation of satellite-derived latent heat fluxes, *J. Clim.*, *10*, 2782–2795, doi:10.1175/1520-0442(1997)010<2782:EOSDLH>2.0.CO;2.

Servain, J., A. J. Busalacchi, M. J. McPhaden, A. D. Moura, G. Reverdin, M. Vianna, and S. E. Zebiak (1998), A pilot research moored array in the tropical Atlantic (PIRATA), *Bull. Am. Meteorol. Soc.*, *79*(10), 2019–2031, doi:10.1175/1520-0477(1998)079<2019:APRMAI>2.0.CO;2.

Shay, L. K., G. J. Goni, and P. G. Black (2000), Effects of a warm oceanic feature on Hurricane Opal, *Mon. Weather Rev.*, *128*, 1366–1383, doi:10.1175/1520-0493(2000)128<1366:EOAWOF>2.0.CO;2.

Smith, S. D. (1988), Coefficients for sea surface wind stress, heat flux, and wind profiles as a function of wind speed and temperature, *J. Geophys. Res.*, *93*(C12), 15,467–15,472, doi:10.1029/JC093iC12p15467.

Smith, S. R., D. M. Legler, and K. V. Verzone (2001), Quantifying uncertainties in NCEP reanalyses using high-quality research vessel observations, *J. Clim.*, *14*, 4062–4072, doi:10.1175/1520-0442(2001)014<4062:QUINRU>2.0.CO;2.

Smith, S. R., P. J. Hughes and M. A. Bourassa, (2010), A comparison of nine monthly air-sea flux products, *Int. J. Climatol.*, *31*, 1002–1027, doi:10.1002/joc.2225.

Taylor, P. K., and M. A. Yelland (2000), On the apparent "imbalance" term in the turbulent kinetic energy budget, *J. Atmos. Oceanic Technol.*, *17*, 82–89, doi:10.1175/1520-0426(2000)017<0082:OTAITI>2.0.CO;2.

Wang, C., D. B. Enfield, S.-K. Lee, and C. W. Landsea (2006), Influences of the Atlantic Warm Pool on Western Hemisphere summer rainfall and Atlantic hurricanes, *J. Clim.*, *19*, 3011–3028, doi:10.1175/JCLI3770.1.

Wang, J., H. L. Cole, D. J. Carlson, E. R. Miller, K. Beierle, A. Paukkunen, and T. K. Laine (2002), Corrections of humidity measurement errors from the Vaisala RS80 radiosonde—Application to TOGA COARE data, *J. Atmos. Oceanic Technol.*, *19*, 981–1002, doi:10.1175/1520-0426(2002)019<0981:COHMEF>2.0.CO;2.

Wentz, F. J. (1997), A well-calibrated ocean algorithm for SSM/I, *J. Geophys. Res.*, *102*, 8703–8718, doi:10.1029/96JC01751.

Yu, L., R. A. Weller, and B. Sun (2004), Improving latent and sensible heat estimates for the Atlantic Ocean (1988–99) by a synthesis approach, *J. Clim.*, *17*, 373–393, doi:10.1175/1520-0442(2004)017<0373:ILASHF>2.0.CO;2.

Yu, L., X. Jin, and R. A. Weller (2006), Role of net surface heat flux in seasonal variations of sea surface temperature in the tropical Atlantic Ocean, *J. Clim.*, *19*, 6153–6169, doi:10.1175/JCLI3970.1.

Yu, L., X. Jin, and R. A. Weller (2008), Multidecade global flux datasets from the Objectively Analyzed Air-Sea Fluxes (OAFlux) Project: Latent and sensible heat fluxes, ocean evaporation, and related surface meteorological variables, *OAFlux Proj. Tech. Rep. OA-2008–01*, Woods Hole Oceanogr. Inst., Woods Hole, Mass.

Zeng, X., M. Zhao, and R. E. Dickinson (1998), Intercomparison of bulk aerodynamic algorithms for the computation of sea surface fluxes using TOGA COARE and TAO data, *J. Clim.*, *11*, 2628–2644, doi:10.1175/1520-0442(1998)011<2628:IOBAAF>2.0.CO;2.

Zhang, F. W., W. M. Drennan, B. K. Haus, and H. C. Graber (2009), On wind-wave-current interactions during the Shoaling Waves Experiment, *J. Geophys. Res.*, *114*, C01018, doi:10.1029/2008JC004998.

A. Bentamy, Institut Francais de Recherche pour l'Exploitation de la Mer, BP 70, F-29280 Plouzane, France.

J. A. Carton, R. T. Pinker, and A. Santorelli, Department of Atmospheric and Oceanic Science, University of Maryland, College Park, MD 20742, USA.

W. M. Drennan and K. B. Katsaros, Rosenstiel School of Marine and Atmospheric Science, University of Miami, 4600 Rickenbacker Cswy., Miami, FL 33149, USA. (katsaros@whidbey.net)

A. M. Mestas-Nuñez, Department of Physical and Environmental Sciences, Texas A&M University-Corpus Christi, 6300 Ocean Dr., Corpus Christi, TX 78412, USA.